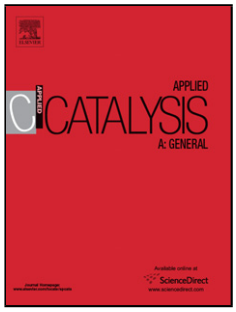

Title: Ni/HZSM-5 catalyst preparation by deposition-precipitation. Part 2. Catalytic hydrodeoxygenation reactions of lignin model compounds in organic and aqueous systems

Authors: R.R. Barton, M. Carrier, C. Segura, J.L. Garcia Fierro, S. Park, H.H. Lamb, N. Escalona, S.W. Peretti

PII: S0926-860X(18)30288-6
DOI: https://doi.org/10.1016/j.apcata.2018.06.012
Reference: APCATA 16700

To appear in: *Applied Catalysis A: General*

Received date: 5-2-2018
Revised date: 5-6-2018
Accepted date: 7-6-2018

Please cite this article as: Barton RR, Carrier M, Segura C, Garcia Fierro JL, Park S, Lamb HH, Escalona N, Peretti SW, Ni/HZSM-5 catalyst preparation by deposition-precipitation. Part 2. Catalytic hydrodeoxygenation reactions of lignin model compounds in organic and aqueous systems, *Applied Catalysis A, General* (2018), https://doi.org/10.1016/j.apcata.2018.06.012

Ni/HZSM-5 Catalyst Preparation by Deposition-Precipitation. Part 2. Catalytic Hydrodeoxygenation Reactions of Lignin Model Compounds in Organic and Aqueous Systems

R. R. Barton[a], M. Carrier[b,1], C. Segura[c], J. L. Garcia Fierro[d], S. Park[e], H. H. Lamb[a], N. Escalona[f,g,h], S.W. Peretti[a]

[a]North Carolina State University, Department of Chemical and Biomolecular Engineering, Raleigh, NC
[b]Universidad de Concepción, Unidad de Desarrollo Tecnológico, Coronel, Chile.
[1]European Bioenergy Research Institute, Aston University, Birmingham B4 7ET, UK.
[c] Unidad de Desarrollo Tecnológico, Universidad de Concepción, Coronel, Chile.
[d]Instituto de Catálisis y Petroquímica, CSIC, Cantoblanco, 28049 Madrid, Spain.
[e]North Carolina State University, Department of Forest Biomaterials, Raleigh, NC
[f]Pontificia Universidad Católica de Chile, Departamento de Ingeniería Química y Bioprocesos, Santiago, Chile.
[g]Pontificia Universidad Católica de Chile, Facultad de Químicas, Santiago, Chile.
[h]Centro de Investigación en Nanotecnología y Materiales Avanzados (CIEN-UC), Pontificia Universidad Católica de Chile, Santiago, Chile.

Ryan R. Barton:
rrbarton@ncsu.edu

Marion Carrier:
m.carrier@aston.ac.uk

Cristina Segura:
c.segura@udt.cl

Jose Luis Garcia Fierro:
jlgfierro@icp.csic.es

Sunkyu Park:
sunkyu_park@ncsu.edu

H. Henry Lamb:
lamb@ncsu.edu

Néstor Escalona:
neescalona@ing.puc.cl

Corresponding Author:
Steven W. Peretti
Department of Chemical and Biomolecular Engineering, NC State University
Campus Box 7905
Raleigh, NC 27695-7905
peretti@ncsu.edu

Graphical abstract

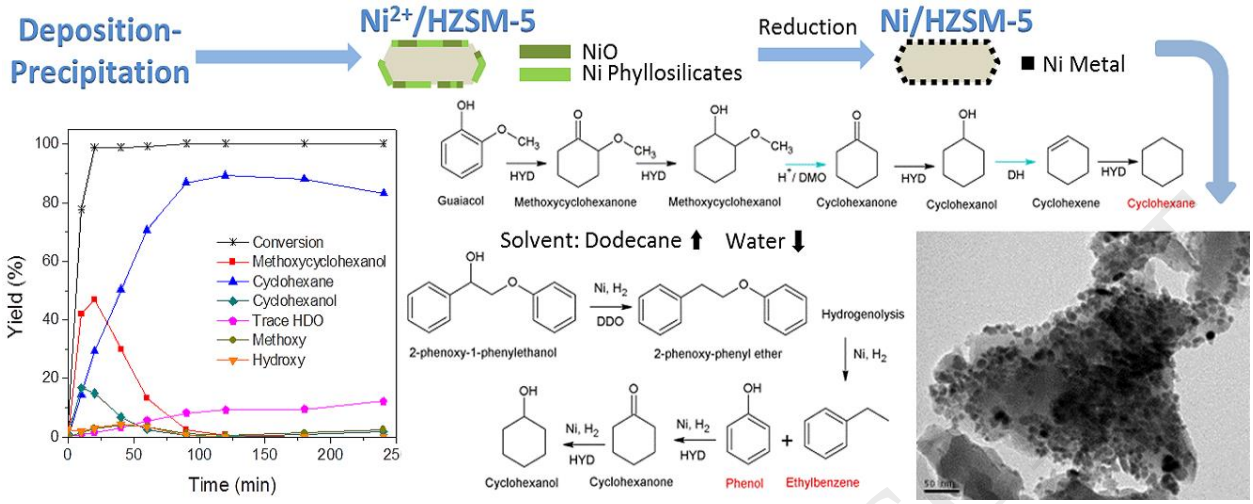

Highlights

- Effect of catalyst properties of Ni/HZSM-5 synthesized via excess deposition-precipitation times on guaiacol and 2-phenoxy-1-phenylethanol hydrodeoxygenation was studied.
- Ni(15)/HZSM-5 with 16 h DP time and calcined at 673 K had high intrinsic rates and high selectivity.
- Selectivity towards aromatic products was highest in neutral aqueous environments.
- Ni/HZSM-5 from deposition-precipitation is a promising catalyst for lignin cleavage at low temperature.

Abstract

Nickel metal supported on HZSM-5 (zeolite) is a promising catalyst for lignin depolymerization. In this work, the ability of catalysts prepared via deposition-precipitation (DP) to perform hydrodeoxygenation (HDO) on two lignin model compounds in organic and aqueous solvents was evaluated; guaiacol in dodecane and 2-phenoxy-1-phenylethanol (PPE) in aqueous solutions. All Ni/HZSM-5 catalysts were capable of guaiacol HDO into cyclohexane at 523 K. The role of the HZSM-5 acid sites was confirmed by comparison with Ni/SiO_2 (inert support) which exhibited incomplete deoxygenation of guaiacol due to the inability to perform the cyclohexanol dehydration step. The catalyst prepared with 15 wt% Ni, a DP time of 16 h, and a calcination temperature of 673 K (Ni(15)/HZSM-5 DP16_Cal673), performed the guaiacol conversion with the greatest selectivity towards HDO products, with an intrinsic rate ratio (HDO rate to conversion rate) of 0.31, and 90% selectivity to cyclohexane**.** Catalytic activity and selectivity of Ni/HZSM-5 (15 wt%) in aqueous environments (water and 0.1 M NaOH solution) was confirmed using PPE reactions at 523 K. After 30 min reaction time in water, Ni/HZSM-5 exhibited ~100% conversion of PPE, and good yield of the desired products; ethylbenzene and phenol (~35% and 23% of initial carbon, respectively). Ni/HZSM-5 in NaOH solution resulted in

significantly higher ring saturation compared to the Ni/HZSM-5 in water or the NaOH solution control.

Keywords: hydrodeoxygenation; lignin; depolymerization; HZSM-5; deposition-precipitation

1. Introduction

Pulp and paper plants, and lignocellulosic biorefineries, generate lignin residues as a byproduct stream. Rather than burn it to power industrial processes [1-7], if successfully depolymerized, it could be used to produce aromatic compounds, platform chemicals, and other high value, petroleum-based products [2-5]. The strategy taken in this work is the depolymerization of lignin into simple aromatic monomers through the use of a bifunctional catalyst, one capable of hydrogenolysis of both C-O and C-C linkages in lignin, under mild reaction conditions in an aqueous environment. Two model compounds were chosen to probe catalyst hydrodeoxygenation (HDO activity); guaiacol and 2-phenoxy-1-phenylethanol (PPE). Guaiacol exhibits an aromatic ring with C-O bonds in the form of methoxy and hydroxy moieties which are more accessible than the β-O-4 linkage present in PPE. Successful hydrodeoxygenation of these compounds would establish this catalyst as a promising candidate for depolymerization of the more complex lignin molecule.

To evaluate the catalyst performance, a preliminary high-throughput screening based on guaiacol HDO assays is used. The C-O bonds in the form of methoxy and hydroxy moieties all can undergo hydrogenolysis; cleavage via hydrodeoxygenation is an effective form of hydrogenolysis for the depolymerization of lignin. In this work, a series of Ni/HZSM-5 catalysts which were synthesized via deposition-precipitation (DP) and characterized previously [8] are evaluated vis-a-vis the hydrodeoxygenation (HDO) of guaiacol, a lignin model compound. In an additional study, the developed catalyst was evaluated with a lignin model compound in various aqueous media which serve as environmentally friendly alternatives to organic solvents.

This strategy has been proven to be successful as reported in two recent studies using Ni/HZSM-5, prepared via incipient wetness impregnation (IWI), in an aqueous environment for the HDO of phenol (5 MPa H_2, 473 K, 3 h reaction time, using 7-9 wt% nickel), and for the upgrading of pyrolysis oil and various aromatic monomers and dimers (5 MPa H_2, 523 K, 2 h for phenol and 4 h for pyrolysis oil, using 20 wt% nickel) [9, 10]. For all the reactions performed in the aqueous environment, a high extent of HDO was observed, with mainly C-O cleavage and some aromatic ring saturation. Reactions involving phenol over 3 h resulted in 80-100% conversion, with 90-100% selectivity to cyclohexane. Other aromatic monomers had 90-100% conversion, with approximately 90% selectivity to hydrocarbons and about 10% to methanol. Of the 90%, 75-90% were cycloalkanes and 5-15% were aromatics. For the dimer reactions, 100% conversion was achieved, with only 18-37% of aromatics yielded, and for the pyrolysis oil, 100% deoxygenation was achieved, with 10% paraffins, and 90% cycloalkanes and aromatics. As shown from the studies of nickel catalyzed HDO reactions in aqueous environments, supported nickel catalysts, such as Ni/HZSM-5, exhibit promise for the selective cleavage of C-O linkages that represent the dominant bonds in lignin [2]. However, the studies mentioned above only used nickel catalysts prepared with IWI techniques and not DP, which is the focus of this work.

Song *et al*. [11] compared 5wt% Ni/Hβ catalysts prepared by 4 different techniques, including IWI and DP. They found that the Ni/Hβ prepared by the DP method not only had the smallest particle size and tightest particle size distribution (highest dispersion nickel catalyst), it also had the fastest rate of stearic acid HDO and displayed high stability after multiple reaction runs [11]. He *et al*. [12, 13] produced Ni/SiO_2 using the DP method for the cleavage of β-O-4, α-

O-4, and 4-O-5 aromatic ether dimers in an aqueous phase (393 K, 0.6 MPa H_2, 40-57 wt% nickel, and 90 min reaction time). Both studies observed selective cleavage of the ether bonds, along with some aromatic ring saturation. These studies were only looking at Ni/SiO_2, and not the multifunctional Ni/HZSM-5 system [12, 13].

Song *et al*. [14] prepared Ni/HZSM-5 catalyst by the DP method for the HDO of several substituted phenols (473 K, 3 MPa H_2, 20 wt% nickel, and 0-2 h reaction time) in an aqueous environment and proposed several reaction pathways. That catalyst system successfully performed HDO, and, more specifically, C-O hydrogenolysis. The role of the acidic support in the adsorption of the reactants for hydrogenolysis instead of aromatic ring hydrogenation was also reported [14]. Each study used the DP procedure that was developed and characterized by Burattin *et al*. [15, 16] to prepare a Ni/SiO_2 catalyst. In this laboratory [8], a different DP procedure was utilized. Nickel loading was manipulated by varying the concentration of nickel nitrate, rather than the DP time. The effects of catalyst preparation conditions and resulting catalyst properties on HDO activity were then characterized.

Catalyst activity and selectivity were evaluated using a guaiacol HDO reaction in n-dodecane solvent, a commonly used reaction assay [17-20]. Guaiacol serves as a simple model compound for depolymerized lignin due to the presence of the aromatic ring and the substituent methoxy and hydroxy groups, which are common in the lignin structure. This model reaction system was used for several reasons: a) to avoid complicated effects of a multiphase liquid system, b) to avoid effects of the aqueous phase on the support and on the activity of the nickel catalyst [21, 22], and c) to simplify the product analysis by limiting the number of chemical species present in the reaction system. Once kinetic and catalytic, properties were assessed, it was necessary to establish the role of the HZSM-5 support and the global catalytic activity Ni/HZSM-5 in diverse aqueous reaction environments (e.g. neutral and alkaline aqueous solutions). Aqueous environments have been observed to preserve aromaticity (at the cost of slower reaction rates) with similar kinds of lignin model compounds [21, 23]. Water will not solubilize lignin, but it prevents significant ring saturation. Using a NaOH solution as a solvent has also been shown to have positive effects on lignin depolymerization. It solubilizes lignin, allowing the lignin to be more dispersed in the reaction mixture, reducing char formation, and it hydrolyzes lignin through base catalysis [24, 25]. For these reasons, 2-phenoxy-1-phenylethanol (PPE) was used as a lignin model compound in aqueous environments to further demonstrate the activity of the Ni/HZSM-5 produced by this modified DP procedure; specifically, its ability to cleave β-O-4 linkages found in lignin.

Effective catalysts exhibit high activity and high selectivity for HDO products. This should coincide with favorable nickel particle characteristics, including high dispersion. The catalyst with the greatest selectivity for HDO from this simple model system will be used against other model lignin compounds and lignin in aqueous solvents in subsequent studies. Nickel loading and catalyst preparation were varied to determine whether the optimal nickel loading found in Barton *et al.* [8] correlates with the highest intrinsic rate and/or selectivity toward complete deoxygenation. The optimal loading (15 wt% Ni) was defined as the highest loading without significant reduction in dispersion and increase in particle size. In addition, degradation mechanisms were examined and discussed.

2. Experimental

2.1 Catalyst Preparation and Characterization

The Ni/HZSM-5 was synthesized using a DP method similar to that of Burattin *et al*. [15, 16]. For each catalyst preparation, 5 g of catalyst was synthesized with varying nickel loading, 5, 10, 12.5, 15, and 20 wt% nickel. All catalysts are referred to by their nominal loading, based on the initial mass of nickel introduced during synthesis. The resulting nickel levels, measured using ICP-OES, are reported in **Table 1A**, and vary less than 20% from the nominal loading levels.

DP method parameters, including concentration of NH_4-ZSM-5 support (Zeolyst International, CBV 2314), urea, nitric acid, temperature, stirring, and DP time, were kept constant. Unlike the standard method, which uses excess amounts of nickel nitrate and varies the DP time to control the nickel loading, the nickel loading was controlled by using an initial concentration of nickel nitrate corresponding to the total amount of nickel desired for each catalyst, and then using a constant, excess DP time to incorporate the nickel. The following concentrations were used to synthesize the catalyst samples: 7.9 g NH_4-ZSM-5·L^{-1} water, 0.42 mol·L^{-1} urea, 0.02 mol·L^{-1} nitric acid, and 0.01-0.03 mol·L^{-1} $Ni(NO_3)_2 \cdot 6H_2O$. All concentrations are based on the total amount of water, which depends on the required amount of support to make 5 g of catalyst of a specific nickel loading. The catalysts discussed in this work were all prepared using the methodology previously developed in this laboratory [8].

The DP method is capable of forming a combination of nickel hydroxide and 1:1 nickel phyllosilicate species on the support [13-16, 26]. During calcination, the nickel hydroxide decomposes into NiO, and the 1:1 nickel phyllosilicate forms 2:1 nickel phyllosilicate. He *et al*. [12] related TOF by Ni/SiO_2 to calcination temperature and particle size. The data suggests that calcination temperature may contribute to a more complete transformation of a nickel-support species during calcination, followed by a greater extent of reduction to nickel metal prior to the reaction. For this reason, all catalyst precursors in this study were calcined either at 673 K or 873 K. After calcination, the sample was cooled and then stored for activation. Calcined catalyst samples were then reduced in H_2 gas environment at 733 K. Given that a batch reactor system was used for these experiments, the Ni/HZSM-5 catalyst was exposed to air during loading of the reaction vessel, causing re-oxidation of the nickel metal [27, 28]. To prevent extensive oxidation and allow for a systematic and consistent oxygen exposure for all catalyst samples, catalysts underwent passivation to form an oxidized surface layer on the nickel metal [8], which could then be reduced in the reactor vessel *in-situ* under the reaction conditions. After passivation, the catalysts were stored in a desiccator at room temperature for future reactions and catalyst characterization All synthesized catalysts were characterized via various techniques as detailed in Barton *et al.* [8]. The techniques applied include:

(1) Nitrogen adsorption-desorption isotherms to determine BET surface areas, total pore volumes, micropore volumes (Dubinin-Radushkevich model), micropore size distributions (carbon dioxide adsorption isotherms, DFT model), and mesopore size distributions (BJH model);
(2) Inductively coupled plasma-optical emission spectrometer (ICP-OES) to determine Si/Al ratios of the HZSM-5 support and nickel loading of the catalysts;

(3) Temperature programmed reduction (TPR) to determine H_2/Ni uptake over increasing temperature and confirm complete reduction of the nickel catalysts;
(4) X-ray diffraction (XRD) to determine the types of nickel species present in the nickel catalysts and to estimate nickel particle diameter via the Scherrer equation (Eq. (1)), where D_p is particle diameter (Å), λ is CuKα radiation wavelength (Å), $\beta_{1/2}$ is the full width at half maximum (radians), and θ (Bragg angle) is the position (1/2 value of 2θ position) (radians);
(5) Transmission electron microscopy (TEM) to determine mean nickel particle sizes and distributions;
(6) H_2-chemisorption to determine available nickel sites, dispersion (%) calculated by Eq. (2) where D is the dispersion in %, H atoms is the amount of hydrogen atoms in mmol based on the volume of H_2 chemisorbed, and Ni is the amount of nickel in mmol based on the nickel loadings determined by ICP-OES, and approximate nickel particle size using Eq. (3), where d_p is particle diameter in nm and D is the dispersion in %, which assumes that a spherical particle that is less than 1 nm in diameter exhibits 100% dispersion [29];
(7) Acid strength of the HZSM-5 support with and without nickel was measured using a potentiometric titration method [30]; and
(8) X-ray photoelectron spectroscopy (XPS) was used to observe surface species of the supported nickel catalysts.

Important characteristic data relevant to this work have been included in **Tables 1 – 2** [8].

$$D_p = \frac{0.94\lambda}{\beta_{1/2} cos\theta} \quad (1)$$

$$D = 100 * \frac{H\ atoms\ (mmol)}{Ni\ (mmol)} \quad (2)$$

$$d_p = \frac{101}{D\ (\%)} \quad (3)$$

While the catalyst preparation for the guaiacol HDO reactions is identical to the methods used in Barton *et al.* [21], the catalyst applied to PPE model compound reactions had slightly different preparation conditions, which include: 7.6 g·L^{-1} HZSM-5 (instead of 7.9 g·L^{-1}), 0.02 M $Ni(NO_3)_2 \cdot 6H_2O$ (within the range used for previously) in 560 mL of water, and a DP time of 16 h was used. Due to use of an alternate lab with different equipment and capabilities, calcination was performed at 673 K for 4 h with a 5 K·min^{-1} ramp. Approximately 0.5 g of calcined catalyst was reduced in a quartz reactor tube connected to a flow system. The tube was first purged with N_2 at 63 mL·min^{-1} for 10 min. H_2 gas was then flown into the reactor at 7 mL·min^{-1} for a total of 70 mL· min^{-1} (10% v/v H_2). After flowing the mixture for 5 min, the reduction oven program was initiated. The catalyst was reduced at 733 K for 4 h with a 2.5 K·min^{-1} ramp. After reduction, the reactor tube was purged with N_2 gas flow at 63 mL·min^{-1} and allowed to cool to room temperature. Once the system cooled, the gas flows were shutoff, and the reactor tube fittings were loosened to allow slow exposure to air overnight. After passivation, the catalyst was removed from the apparatus and stored for reactions and catalyst characterization. The properties of the Ni/HZSM-5 catalyst used in this work are listed in **Table 3** and its TPR profile, XRD

patterns, and TEM/SEM images are presented in **Figs. S1, S2**, **S3** respectively (this catalyst corresponds to the Ni(15)/HZSM-5 - DP16_Cal673 catalyst in **Tables 1B** and **2B)**.

2.2 Reagents and Model Compound Preparation

The catalysts were evaluated with three different reaction environments. The first reaction assay was a guaiacol HDO reaction using a batch reactor system with the non-polar solvent, n-dodecane, and n-hexadecane as an internal standard. All these compounds were purchased (n-dodecane (Merck Millipore, ≥99.0%), guaiacol (Merck Millipore, ≥98%), and n-hexadecane (Sigma Aldrich, 99%).

The second and third reaction assays were a PPE β-O-4 cleavage reaction using a batch reactor system with water and 0.1 M sodium hydroxide (Fisher Chemical, ≥97%) solution as the solvent. The PPE was prepared via a synthesis method consisting of two main steps. The first step was a combination reaction between 2-bromoacetophenone (Acros Organics, 98%) and phenol (Aldrich, 99.99%) to form 2-phenoxyacetophenone. The second step reduced the 2-phenoxyacetophenone to form PPE. The complete synthesis procedure is provided in **Fig. S4** [31]. This procedure produced a white solid with an overall yield of 70% (1:1 stoichiometry between moles of initial limiting reagent, 2-bromoacetophenone, and PPE). The identity was confirmed by GC-MS (**Fig. S5**), and by comparison with a commercially purchased PPE using GC-FID (**Fig. S6**). To also confirm the purity of the synthesized PPE, TGA-DSC (SDT Q600 TA Instruments) was used to compare heat flow versus temperature data which confirmed that both the purchased PPE and the synthesized PPE exhibited a phase change (melting point) at the same temperature and were calculated to have similar purities >97% (based on TA Universal Analysis software) (**Fig S7**).

2.3 Catalytic Performance

2.3.1 Guaiacol/Dodecane System

The reactions were performed in a 300 mL Parr reactor equipped with a gas entrainment impeller and baffle, thermocouple, heating jacket, inlet gas line valve, and outlet liquid sampling valve with a filter to prevent loss of solid catalyst. Each reaction used dodecane (80 mL), guaiacol (0.28 $mol \cdot L^{-1}$), n-hexadecane (0.03 $mol \cdot L^{-1}$, internal standard), and Ni(x)/HZSM-5 catalyst (0.05 g, calcined, reduced, and passivated). The reaction was performed at 523 K under 5 MPa of H_2 gas for 4 h. Samples were taken at the start of the reaction (time = 0 min is when H_2 gas was introduced to the reactor after reaching the reaction temperature), 10 min, 20 min, 40 min, 1 h, 1.5 h, 2 h, 3 h, and 4 h. Along with reactions using Ni/HZSM-5, a reaction with Ni/SiO_2 was also performed to observe the influence of the HZSM-5 acid support versus the inert SiO_2 (Strem, 99+%) support.

Samples were quantified using GC-FID. Product identification was determined using a combination of GC-MS results and reference samples in the GC-FID to confirm residence times. A PerkinElmer Clarus 400 GC-FID was utilized, and equipped with a CP-SIL 5 Agilent column (30 m x 0.53 mm x 1.0 μm). The GC-MS utilized was a PerkinElmer Clarus 680 equipped with an Elite-1 PerkinElmer column (30 m x 0.32 mm x 0.25 μm). The carrier gas flow was 50

mL/min, with an injector temperature of 548 K and split ratio of 20:1. The GC oven program started with a 6 min hold at 305 K, followed by heating to 343 K at 30 K/min and a hold for 22 min, then heating to 548 K at 30 K/min and a hold at for 3 min. After peak assignments using GC-MS and reference samples, the n-hexadecane internal standard was used to quantify confirmed HDO products. The FID detector temperature was set at 453 K with a hydrogen flow rate of 45 mL/min and an air flow rate of 450 mL/min. The detector response is proportional to the concentration of the compounds observed and therefore used directly to determine yields. In addition, the internal standard peak and total peak areas were used to confirm consistency among samples and track the fate of the starting guaiacol.

Results from GC-FID analysis of reaction time course samples were used to calculate specific rates for guaiacol conversion and HDO rates (rate of producing completely deoxygenated products; i.e., cyclohexane, cyclohexene, methylcyclopentane, and trace benzene). Specific rates are normalized per gram of nickel, as determined from ICP-OES results, which are displayed in **Table 1A** and **B**. Specific (per gram of nickel basis) and intrinsic (per nickel site basis) initial rates are calculated from the slope of the linear region of guaiacol conversion (per catalyst) over time (within the first 50min of reaction) and are synonymous with guaiacol conversion rates. The turnover frequencies (TOF) for guaiacol conversion and HDO generation were made intrinsic using the calculated specific rates and the number of active nickel sites, as determined from H_2-chemisorption dispersion results (which gives the total number of sites if 100% of nickel is reduced). As discussed in Barton *et al.* [8], the XPS results in **Table 2A** and **B** show incomplete reduction of the nickel sites; however this was attributed to minor exposure of the nickel metal to oxygen prior to the XPS analysis. Given the use of passivation to allow easy in-situ re-reduction, the temperature of the reactions, and the high pressure of H_2 gas utilized, it is reasonable to assume that all the catalysts were fully reduced during the reactions. The intrinsic rate (I_R) of guaiacol conversion in the presence of Ni/HZSM-5 was calculated as follows:

$$I_R = \frac{S_R * N_{av}}{Ni_{SA}} \tag{4}$$

with the specific rate represented by S_R; Avogadro's number represented by N_{av}; and the number of available nickel sites per gram of catalyst (reduced nickel sites) by $Ni_{SA.}$ Calculation of Ni_{SA} is as follows:

$$Ni_{SA} = \frac{Ni_{SC}}{Ni_L} \tag{5}$$

where Ni_{SC} represents the number of nickel sites per gram of catalyst, as determined by H_2-chemisorption, and Ni_L is the nickel loading as determined by ICP-OES.

2.3.2 PPE/Water System

The reactions were performed in a 50 mL Parr reactor equipped with an impeller, a thermocouple, a heating jacket, inlet and outlet gas valves, and a safety rupture disc. Each reaction used 20 mL of water and 0.535 g of PPE (0.125 M). HZSM-5 reactions used 0.0535 g of

catalyst (Mobil HZSM-5, 10:1 w/w feed to catalyst), while Ni/HZSM-5 reactions used 0.027 g of Ni/HZSM-5 catalyst (Ni supported on Zeolyst HZSM-5, 20:1 w/w, feed to catalyst). Reactions were performed at 523 K under 5 MPa of H_2 gas for 0-2 h. The H_2 gas was introduced prior to the temperature ramp to 523 K, and the start time was the moment the reactor reached the reaction temperature (autogenous pressure was about 8 MPa). The HZSM-5 reactions were performed for 5 min, 15 min, 0.5 h, 1 h, and 2 h. The Ni/HZSM-5 reactions were performed for 0.25 h, 0.5 h, and 1 h, and a *p*-hydroxyacetophone internal standard was added to the reaction mixture after the reaction, but prior to collection (approximately 8 mg).

For the HZSM-5 reactions, the product mixtures were collected with 20 mL of methanol (Fisher Chemical, HPLC grade), and the products were further diluted using a 1:1 v/v ratio of sample to methanol. The Ni/HZSM-5 reaction mixtures were collected with acetone (EMD Millipore, HPLC grade) (approximately 20 mL, enough acetone added until reaction mixture was a single phase with known total volume). For both reactions, the product mixtures were centrifuged to remove catalyst, and then a 1.5 mL aliquot of the single phase reaction products was taken directly, filtered through a 0.22 μm nylon syringe filter (Fisherbrand™) and then injected into a GC for analysis. The reaction products at each time interval (15-30 min) were quantified using GC-FID. Product identification was determined using a combination of GC-MS results and standards in the GC-FID to confirm compound residence times. The GC-FID used was a Shimadzu GC-2010, with a ZB-5MS Zebron column (30 m x 0.25 mm x 0.25 μm), which is a G27 USP phase column (5% phenyl, 95% dimethylpolysiloxane). The GC-MS used was a Shimadzu GC-2010 paired with a quadrupole mass spectrometer (GCMS-QP2010S), also equipped with a ZB-5MS Zebron column (30 m x 0.25 mm x 0.25 μm). The analysis methods for the GC-FID and GC-MS are provided in **Figs. S8 and S9**, respectively.

2.3.3 PPE/NaOH Solution System

The reactions were performed in a 50 mL Parr reactor equipped with an impeller, a thermocouple, a heating jacket, inlet and outlet gas valves, and a safety rupture disc. Each reaction used 20 mL of 0.1 M NaOH solution and 0.535 g of PPE (0.125 M). Ni/HZSM-5 reactions used 0.027 g of Ni/HZSM-5 catalyst (Ni supported on Zeolyst HZSM-5, 20:1 w/w, feed to catalyst). Reactions were performed at 523 K under 5 MPa of H_2 gas for 0-1 h. The H_2 gas was introduced prior to the temperature ramp to 523 K, and the start time was the moment the reactor reached the reaction temperature (autogenous pressure was about 8 MPa). The reactions were performed for 0.25 h, 0.5 h, and 1 h, and a dodecane internal standard was added to the reaction mixture after the reaction, but prior to collection (0.1 mL).

The alkaline reaction mixtures were collected with water (20 mL), acidified with 2 mL hydrochloric acid (Fisher Chemical, Technical grade), centrifuged to remove catalyst, and extracted with ethyl ether (Fisher Chemical, Laboratory grade) (20 mL, three times) to recover the organics. A 1.5 mL aliquot from the ethyl ether phase (with a known total volume) was filtered through a 0.22 μm nylon syringe filter (Fisherbrand™) and then injected into a GC for analysis using the GC methods stated in section 2.3.2.

3. Results and Discussion

3.1 Guaiacol HDO Activity in Dodecane

3.1.1 Effect of Nickel Loading on Guaiacol HDO

The three main products from the conversion of guaiacol, regardless of nickel loading, were 2-methoxycyclohexanol, cyclohexanol, and cyclohexane, as shown by the reaction progress plots in **Fig. 1**. There were trace amounts of various HDO products (other completely deoxygenated products) as well as partially hydrodeoxygenated compounds containing only methoxy or hydroxy groups. Of all the catalyst loadings, only the 5 wt% nickel catalyst did not reach 100% conversion of guaiacol after 4 h of reaction. As nickel loading increased from 10-20 wt% nickel, the time required to reach 100% conversion decreased. In addition, the amount and rate (as indicated by the slopes of the yield plots) at which cyclohexane and other HDO products (i.e., methylcyclopentane, cyclohexene, and benzene) are formed also increases with nickel loading, and are accompanied by a decrease in the amount and a faster rate of disappearance of 2-methoxycyclohexanol, cyclohexanol, and other oxygenated compounds.

The specific rates for guaiacol conversion and HDO production both reach a maximum at 15 wt% nickel loading, as shown in **Fig. 2a**. The decrease in rate for the 20 wt% catalyst suggests that less of the nickel is available for reaction sites, consistent with the hypothesis that large aggregate nickel particles were formed at higher loading, resulting in lower surface area (**Table 1A**) and fewer active sites. This is also in accordance with the H_2-chemisorption results (**Table 1A)** showing that the 20 wt% catalyst has lower dispersion than the catalysts with lower nickel loading [8].

The intrinsic rates for all Ni(x)/HZSM-5 catalysts should be unchanging if the structure and local environment of the active nickel sites are equivalent at all nickel loading levels. The intrinsic rates, shown in **Figs. 2b** and **3**, suggest that there are at least two different active site configurations available for HDO activity, and possibly as many as three for guaiacol conversion. In **Fig. 3a**, the intrinsic rate data for the guaiacol conversion indicate a dramatic change in the activity between the 5-10 wt% region and the 12.5-15 wt% region. Above the 12.5-15 wt% region, the activity of the nickel sites noticeably decreases. This suggests that the active sites are similar for 12.5-15 wt% catalysts (for at least hydrogenation activity), with less active sites on the 5, 10, and 20 wt% nickel catalysts.

In **Fig. 3b**, the low loading asymptote and the apparent high loading level asymptote suggest, qualitatively, the presence of two different catalytic nickel sites. The results at 12.5 wt% Ni could suggest the occurrence of a mixture of the two hypothesized sites. This suggests that the 5-10 wt% catalysts had similar HDO activity, and the 15-20 wt% catalysts had similar HDO activity. The 15 wt% catalyst was in the higher activity region for both guaiacol conversion and HDO intrinsic rates.

Previously hypothesized reaction networks surrounding hydrodeoxygenation with Ni-HZSM-5 catalysts [14, 32, 33] were adapted to reflect the observed products (including trace products) and are presented in **Fig. 4**. The main reaction pathways are presented in part a) and alternate pathways in part b); both are comprised of nickel catalyzed and acid catalyzed reaction steps.

The dominant pathway is highlighted by the dark red pathway in **Fig. 4a**. Hydrogenation/saturation of the aromatic ring occurs first, converting guaiacol to 2-methoxycyclohexanol. The 2-methoxycyclohexanol then undergoes demethoxylation to form cyclohexanol. The cyclohexanol is then converted to cyclohexene via dehydration, followed by hydrogenation to cyclohexane. This pathway is proposed due to the large amounts of 2-methoxycyclohexanol, cyclohexanol, and cyclohexane observed in the reaction products, as well as the reaction progress over time, which first shows formation of 2-methoxycyclohexanol and cyclohexanol, then formation of cyclohexane. The other reactions in the network are not included, as most of the other products are present only in trace amounts.

Fig. 5 shows the product distribution at 20% conversion. The 5 wt% nickel catalyst is not shown because the reaction did not reach 20% conversion within the initial rate region of the reaction progress. As the nickel loading increases, the product distribution shifts, exhibiting a decrease in the formation of 2-methoxycyclohexanol and an increase in the formation of cyclohexane, while the yield of cyclohexanol remains relatively similar between the catalysts. This suggests that increased nickel loading impacts the chemistry of the active site, which is directly reflected by different selectivity towards various types of hydrodeoxygenation and hydrogenolysis (i.e., demethoxylation and direct deoxygenation).

This change in the nature of the active site agrees with the change observed in the intrinsic rate (**Fig. 3b**). For lower nickel loading, the reaction pathway mostly follows the main reaction pathway shown in **Fig. 4a** (dark red pathway). However, as the nickel loading increases, the amount of 2-methoxycyclohexanol formed is reduced. This indicates two possibilities: (1) the conversion rate of 2-methoxycyclohexanol on the active site is increased; or (2) there are other pathways that bypass the formation of 2-methoxycyclohexanol, but still form cyclohexanol and cyclohexane. The data would be consistent with (1) only if going from 12.5% loading to higher loadings caused all of the activities downstream of methoxycyclohexanol (DMO, DH, and HYD) to increase in a coordinated manner, while not affecting the initial hydrogenation activity to the same extent. Since the methoxycyclohexanol production reaches a lower maximum and a higher rate of disappearance with increasing nickel loading (**Fig. 1**), along with changes in product distribution at the same extent of conversion (**Fig. 5**), the existence of alternate pathways is more likely. One potential pathway that does not form 2-methoxycyclohexanol is shown in **Fig. 4b** (purple pathway). This reaction pathway starts with demethylation (DME) of guaiacol to catechol, followed by a hydrogenation (HYD) to 1,2-cyclohexanediol. The cyclohexanediol then undergoes direct deoxygenation (DDO) to cyclohexanol. From cyclohexanol, the reaction follows the same reaction pathway as the main reaction pathway going through a dehydration (DH) of cyclohexanol to form cyclohexene followed by hydrogenation to cyclohexane. As mentioned previously, such a pathway still produces cyclohexanol and cyclohexane without the initial formation of 2-methoxycyclohexanol.

Another possible reaction pathway is shown in **Fig. 4b** (green pathway). In this pathway, guaiacol undergoes direct deoxygenation (DDO) to form anisole; the anisole is hydrogenated forming methoxycyclohexane, and the methoxycyclohexane forms cyclohexane via demethoxylation (DMO). This pathway bypasses 2-methoxycyclohexanol and cyclohexanol formation and could occur along with the main reaction mechanism in **Fig. 4a**. The fact that at 20% conversion the cyclohexanol yield remains constant, while there is a decrease in 2-methoxycyclohexanol yield and an increase in cyclohexane, is consistent with a shift from the

main mechanism in **Fig. 4a** (dark red pathway) to the alternate mechanism in **Fig. 4b** (purple pathway). This shift occurs with increasing nickel loading and corresponds to a shift in nickel species formed during synthesis (**Fig. 6**). Barton *et al.* [8] previously reported that as nickel loading increased, the nickel species formed shifted from a mixture of NiO and nickel phyllosilicate species to predominantly the NiO species that are present after calcination at 873 K.

Besides the qualitative differences in the local environment of the nickel site that result in differing intrinsic rates and reaction pathways, the change in nickel loading had an effect on the specific rates, which are directly related to the dispersion of the nickel particles. The 20 wt% Ni/HZSM-5 catalyst had the fastest rate of formation and highest yield of cyclohexane per mass of catalyst (**Fig. 1e**). However, based on specific rates and, more importantly, on the intrinsic rates, 20 wt% Ni/HZSM-5 catalyst actually had lower guaiacol conversion rates than the 15 wt% Ni/HZSM-5 catalyst, while HDO rates were similar to that of 15 wt%. The decrease in guaiacol conversion rate exhibited is consistent with the idea that the 20 wt% catalyst was composed of larger nickel particles with lower dispersion than the 15 wt% catalyst. Even though there is more nickel present with the higher loading, less nickel surface area is accessible. Therefore, much of the nickel does not participate in the Ni surface-catalyzed reactions. For the nickel loadings less than 20 wt%, which all have similar dispersions, the percentage of total nickel loaded that is available to participate in reactions is similar. When dispersions are similar, the specific rate should increase with nickel loading, since there is proportionally more nickel surface sites available for reaction.

Overall, the Ni(15)/HZSM-5 catalyst had the greatest conversion of guaiacol and rate of HDO. This was not only due to its high metal loading, high dispersion, and small particle size, as was expected from the properties determined from the Barton *et al*. [8] study, but the nickel sites themselves were more active, thus making this concentration of nickel precursor in combination with the corresponding DP method conditions used in this study, the optimal concentration. This observed difference in metallic sites cannot be attributed to electronic effects and varying nickel site coordination which are associated with nickel sites from 1-5 nm, since these nickel particles are in the 10-15 nm size range [34]. An alternative explanation involves the difference in nickel site to acid site ratio which would be expected with varying nickel loading, with an optimal ratio occurring at 15 wt%. The influence of nickel site to acid site ratio on HDO activity is not surprising since previous literature has shown that for supported nickel catalyst systems, HDO efficiency is directly affected by the presence of acidity, and that presence of acid sites adjacent to nickel sites influences the adsorption orientation of substrate molecules on the catalytic sites and consequently the selectivity of the catalyst [14, 35]. Further exploration of the influence of nickel to acid site ratio would require additional quantification of acid sites, however the analytical instrumentation required for this analysis was not available.

3.1.2 Effect of Preparation Conditions on Guaiacol HDO

Fig. 7 shows the reaction progress over time for the four different preparations of Ni(15)/HZSM-5 catalyst. Similar to the Ni(x)/HZSM-5 catalyst experiments, the experiments for Ni(15)/HZSM-5 catalyst with varying preparation conditions all generated the same three main products: cyclohexane, 2-methoxycyclohexanol and cyclohexanol. All experiments reached

~100% conversion after 1 h, with the product distribution changing over the remaining 3 h of reaction.

Catalysts DP5_Cal673, DP5_Cal873, and DP16_Cal873 generated similar results (**Figs.7a**, **7c**, and **7d**), in that a large amount (40-45% yield) of 2-methoxycyclohexanol was formed (along with a minor amount of cyclohexanol), and then these products were gradually consumed and the cyclohexane was gradually formed throughout the reaction. The DP16_Cal673 catalyst, on the other hand, performed differently. The main difference was the much sharper increase and decrease in 2-methoxycyclohexanol, accompanied by a much faster production of cyclohexane (**Fig. 7b**). Other differences include the greater production of HDO products other than cyclohexane, and the reaction being completed within 2 h as opposed to the product distribution changing over the entire 4 h.

The difference in reaction progress between the DP16_Cal673 catalyst and the other catalysts is reflected in **Fig. 8**, which is the product distribution at 20% conversion. The amount of cyclohexane is much higher, while the production of cyclohexanol is much lower, which indicates that an alternate pathway is being favored. In general, all the reactions appear to be following the same main pathway as indicated in **Fig. 4a**. Catalyst DP16_Cal673 however appears to catalyze the alternate pathway shown in **Fig. 4b** (green pathway) to a greater extent, producing cyclohexane without producing cyclohexanol. In addition, more HDO products other than cyclohexane are being formed towards the end of the reaction, which suggests that the acid catalyzed step in **Fig. 4a** toward methylcyclopentane is also more favorable.

The specific initial rates for the four Ni(15)/HZSM-5 catalysts, shown in **Fig. 9a**, were within 2.5-3.5x10^{-3} mol·g Ni^{-1}·s^{-1}, which is reflected by their similar reaction progress over time **(Fig.7)**. However, as reflected by the reaction progress of the DP16_Cal673 catalyst, the specific HDO rate for this catalyst was slightly higher. Unexpectedly, the DP5_Cal673 catalyst had a higher specific initial rate, but this can be attributed to the slightly faster production of 2-methoxycyclohexanol and cyclohexanol during the beginning of the reaction. Despite this, the DP16_Cal673 catalyst still had the highest HDO rate.

The DP16_Cal673 catalyst exhibits the greatest selectivity towards HDO activity of the catalysts evaluated in this study can be inferred from two distinct data sets. The DP16_Cal673 catalyst clearly exhibits the most rapid production and highest yield of cyclohexane (90%), as shown in **Fig. 7b**. While it had the lowest overall intrinsic initial rate, as shown in **Fig. 9b.**, its HDO rate was similar to the other catalysts, resulting in the largest ratio of HDO rate to conversion rate (**Table 4**).

As mentioned in section 2.3.1, the extent of reduction was considered 100% for these catalysts. This is a valid assumption despite what the XPS data in **Table 2B** indicate, because as can be seen in **Fig. 10**, the DP16 catalysts require less severe conditions to be reduced than the DP5 catalysts. Also, the catalysts were passivated, which facilitates in-situ re-reduction. The lower overall intrinsic rate of the DP16 catalysts compared to the DP5 catalysts can be attributed to the fact that the DP16 catalysts were more selective and proceeded through alternate pathways, as described in this section. Overall, the DP16_Cal673 catalyst condition led to the highest dispersion and smallest particle size (**Table 1B**), as well as the most selective catalyst site for HDO. This time the nickel site to acid site ratio should be similar for these catalysts, but in this case the DP16_Cal673 catalyst had nickel particle sizes in the upper limit of 5 nm where electronic effects and different nickel atom coordination may differ from the other 15 wt%

catalyst with larger particle size and this may contribute to the difference in observed selectivity [34].

3.1.3 Effect of Active HZSM-5 versus Inert SiO_2 Support on Guaiacol HDO

To determine the contribution of HZSM-5 support to the catalyst activity, reaction experiments with a Ni/HZSM-5 catalyst and a comparable Ni/SiO_2 catalyst were performed. The nickel loading was reduced for the Ni/SiO_2 preparation to make the ratio of nickel mass to available BET surface area equal, since the SiO_2 has about half the starting surface area of HZSM-5, ~198 $m^2 \cdot g^{-1}$.

The Ni/HZSM-5 catalyst used was a 15 wt% DP16_Cal673 catalyst, and the Ni/SiO_2 was a 7 wt% DP16_Cal673 catalyst (TPR patterns of Ni/SiO_2 compared to Ni/HZSM-5, and BJH mesopore size distributions for Ni/HZSM-5 and Ni/SiO_2 are provided in the Supplementary Material (**Figs. S10** and **S11**, respectively). As can be seen from the reaction progresses displayed in **Fig. 11**, the different supports result in catalysts exhibiting markedly different behavior. With the Ni/HZSM-5, the main products are cyclohexane and HDO products, along with production and consumption of 2-methoxycyclohexanol and cyclohexanol. However, with the Ni/SiO_2, the main products are 2-methoxycyclohexanol along with some cyclohexanol; the extent of HDO of guaiacol does not achieve 100%.

The reaction progress for both reactions is consistent with the proposed mechanism in **Fig. 4a**. Both reactions follow the nickel catalyzed step of aromatic ring saturation to 2-methoxycyclohexanol. While the Ni/HZSM-5 is able to perform acid catalysis to form cyclohexane or methylcyclopentane from 2-methoxycyclohexanol, the Ni/SiO_2 has no acid functionality as confirmed by the absence of acid catalyzed reaction products as indicated in **Fig. 11.** This conclusion is supported by the difference in acid strength exhibited in the potentiometric titration data (**Table 5**).

The presence of cyclohexanol in the Ni/SiO_2 reaction indicates there is an alternate reaction that forms cyclohexanol without forming 2-methoxycyclohexanol, and that pathway was shown in **Fig. 4b** (purple pathway). This pathway starts with 1,2 cyclohexanediol formation, followed by direct deoxygenation to cyclohexanol. However, unlike the Ni/HZSM-5 catalysts, where cyclohexanol undergoes dehydration due to acid catalysis, the Ni/SiO_2 is unable to further convert the cyclohexanol. As mentioned previously, in addition to the main reaction mechanism proposed in **Fig. 4a**, the Ni/HZSM-5 appears to undergo the mechanism in **Fig. 4b** (green pathway), which completely bypasses the formation of 2-methoxycyclohexanol and cyclohexanol. This mechanism uses solely nickel catalysis, and no direct acid catalysis, therefore one would expect the Ni/SiO_2 to also be able to perform this catalytic step and form cyclohexane; however that is not the case as shown from the progress of the Ni/SiO_2 reaction.

This difference in catalytic activity of the nickel may be attributed to the different supports. Even though the purple pathway in **Fig. 4b** does not require acid catalysis, as mentioned in section 1, the presence of acid sites in HZSM-5 adjacent to nickel sites can influence the mechanism of adsorption [11]. The presence of the acid support enables guaiacol to be adsorbed onto the catalytic site in such a way that the catalytic step shown in **Fig. 4b** (green pathway) can be performed. Without the adjacent acid sites, the nickel sites in Ni/SiO_2 are not able to perform the reaction in **Fig. 4b** (green pathway), and instead perform the reactions in **Fig.**

4a and **b** (dark red and purple pathways; without the acid catalyzed steps). Therefore, not only does the Ni/HZSM-5 function as a multifunctional catalyst system with both nickel and acid catalysis, the acid sites adjacent to the nickel sites are able to adsorb guaiacol molecules such that HDO activity is favored.

After demonstrating Ni/HZSM-5 catalyst activity for guaiacol HDO and optimizing its preparation via the DP method, the Ni/HZSM-5 was evaluated in various aqueous environments. The catalytic activities of both, the HZSM-5 support and Ni/HZSM-5 catalyst, were evaluated in neutral and alkaline solutions at the desired reaction conditions (523 K and 5 MPa H_2 gas), specifically for β-O-4 cleavage of 2-phenoxy-1-phenylethanol (PPE).

3.2 PPE β-O-4 Cleavage Activity in Water

When exposed to water and HZSM-5 zeolite, PPE is transformed into two main products as a result of β-O-4 linkage cleavage, phenol and phenylacetaldehyde, along with some dehydration (MW=196 $g \cdot mol^{-1}$) and condensation (MW=222 $g \cdot mol^{-1}$) products (**Fig. 12**). Phenol and phenylacetaldehyde are desirable products, since their presence indicates β-O-4 cleavage of PPE has occurred; dehydration and condensation products are undesirable. The conversion of PPE, yield (wt%) to products, and the selectivity to desired products are presented in **Fig. S12**. In addition to the observed products, there was a systematic loss of approximately 10 wt% (~0.05 g) material that occurred. This loss most likely occurred during collection, including any gaseous products, along with some mass loss due to the dehydration and condensation reactions with the formation of water.

As can be seen from the reaction progress over time (**Fig. 12**), phenol, phenylacetaldehyde, and undesired products are formed during the course of the reaction until the PPE conversion reaches about 100 wt% at around 30 min. After the PPE is completely consumed, between 30 min and 1 h, the phenylacetaldehyde concentration starts to decrease while the undesired product concentration increases. This suggests that there may be a secondary reaction occurring. To test this, reactions with just phenol, phenylacetaldehyde, and the combination of the two were performed under the same conditions. While phenol did not react after 1 h in the reaction system, phenylacetaldehyde did form additional products including the undesired 222 $g \cdot mol^{-1}$ product. The combination of the two formed similar products as in the pure phenylacetaldehyde case, and phenol appeared to be mostly inactive since 95 wt% of the phenol was recovered in the product mixture.

Based on the range of identified products present in the PPE reaction mixture and the side reaction experiments, the reaction mechanisms in **Fig. 13** were proposed. **Fig. 13a** shows the main reaction mechanism where HZSM-5 catalyzes the β-O-4 cleavage of PPE, while **Fig. 13b** shows the suggested mechanism for the formation of undesired products. The presence of phenylacetaldehyde and phenol indicates that acid sites do not simply cleave the ether linkage and form two products in a single step; otherwise only phenol and acetophenone or 1-phenylethanol would have been formed. The exclusive presence of phenylacetaldehyde as opposed to acetophenone suggests that the acid site attacks the ether linkage and releases phenol, but instead of a one-step reaction, there is the formation of an unstable epoxide type ring due to electron propagation from the hydroxide species on the PPE. This oxirane intermediate has the possibility to open up in two ways to form a stable product. The first pathway, the formation of

acetophenone, is the expected one because resonance stability is preserved, therefore more stable than the other possible product of ring opening, phenylacetaldehyde. However, acetophenone is not formed; instead the ring opens via the second path to form the less stable product, phenylacetaldehyde. This suggests that this pathway is kinetically favored, an outcome possibly influenced by the narrow pore size of the catalyst.

The undesired reaction products include a putative result of PPE dehydration (196 $g \cdot mol^{-1}$ from the initial 214 $g \cdot mol^{-1}$), and a higher molecular weight compound (222 $g \cdot mol^{-1}$). Dehydration can be the result of the acid site attacking the hydroxyl group of PPE instead of the ether linkage. The reaction mechanism for the formation of the 222 $g \cdot mol^{-1}$ product is unknown. This uncertainty is mostly due to the inability to identify the product using GC-MS (mass spectra are provided in **Fig. S13**). Despite the unknown product structure and mechanism, from the side reactions discussed above, it is known that the phenylacetaldehyde appears to participate in the reaction to form the 222 $g \cdot mol^{-1}$ product.

From the model reaction with PPE, it has been shown that the HZSM-5 zeolite performs acid catalysis, and with the single catalyst functionality, it is able to cleave the β-O-4 linkage with a selectivity of 68 wt% and yield of 65 wt% to desirable cleavage products (96 wt% conversion of PPE). It was also shown that the HZSM-5 is able to perform the catalysis in an aqueous environment and at a relatively low temperature (523 K), which is quite different from its typical application which is high temperature pyrolysis in the gas phase. The next step was to use the bifunctional catalyst with the presence of nickel metal particles on the HZSM-5 support prepared via the DP method described earlier by Barton *et al.* [8], and compare the activity and selectivity of the Ni/HZSM-5 in water to that of HZSM-5 in water for PPE model compound reactions. The bifunctionality of the Ni/HZSM-5 catalyst was confirmed in section 3.1.3 using guaiacol HDO reactions in dodecane to compare the performance of Ni/HZSM-5 with a Ni/SiO_2 catalyst (inert support). The bifunctional Ni/HZSM-5 catalyst was able to convert guaiacol to cyclohexane, while the Ni/SiO_2 catalyst was only able to convert the guaiacol to cyclohexanol due to inability to perform the acid catalyzed dehydration step from cyclohexanol to cyclohexane.

The results from the Ni/HZSM-5 catalytic reactions against PPE are presented in **Figs. 14a** and **S14**. The Ni/HZSM-5 catalyzed reaction in water exhibited very rapid initial conversion of PPE. The main cleavage products are the desired products, ethylbenzene and phenol; since phenol is an important industrial feedstock and ethylbenzene is a completely deoxygenated aromatic. The production of total monomers again is in the 60-70 wt% range. The control reaction in water without any catalyst exhibits little to no reaction, as shown in **Fig. 14b**. Very little PPE is converted and the reaction is much slower, forming only a small amount of large undesired dimer products that are mainly dehydration products.

The reaction scheme proposed in **Fig. 15** is helpful in understanding the time course of reaction (**Fig. 14a)**. The carbon balance indicates that 2-phenethyl phenyl ether (PPEther) is a reaction intermediate; as suggested by **Fig. 15**, it is the result of PPE undergoing deoxygenation. Subsequent hydrogenolysis of the ether generates ethylbenzene and phenol. Once produced, the ethylbenzene remains in the product mixture without further reaction, whereas the phenol is susceptible to undergo further hydrogenation especially after longer reaction durations. The Ni/HZSM-5 in an aqueous environment demonstrates clearly its ability to generate highly desirable aromatic monomer compounds. It also shows that the nickel metal is in fact active

along with the HZSM-5 support in water, since the reaction mechanisms observed for the Ni/HZSM-5 versus the plain HZSM-5 catalyst (**Figs. 13** and **15**) are quite different. This is in stark contrast with studies described in the literature where non-polar organic solvents are used and ring saturation is predominant [21, 23, 36].

3.3 PPE β-O-4 Cleavage Activity in NaOH Solution

The alkaline PPE cleavage reactions exhibited rapid conversion of PPE (within 15 min) in the presence and absence of catalyst. As shown in **Fig. 16**, the reaction with Ni/HZSM-5 catalyst was able to almost completely convert the PPE in 15 min, and at the 15 min mark, the sample had the largest fraction of aromatic monomers (phenol and methyl benzyl alcohol (MBA)). Following cleavage of the β-O-4 linkage in PPE, the resulting aromatic monomers undergo ring saturation. Phenol was converted to saturated products, including cyclohexanone and cyclohexanol, and the trace aromatics present were also mostly saturated. Only a minor amount of MBA was saturated, but it did appear to undergo a secondary reaction that has not been explored in detail.

The time course of the PPE cleavage reaction, in alkaline solution without catalyst, is shown in **Fig. 16b**. A majority of the PPE was converted within 15 min, though to a lesser extent and yielding a different product distribution than the Ni/HZSM-5 catalyzed reaction. A more detailed comparison of the product yields for the PPE cleavage with and without Ni/HZSM-5 is presented in **Fig. S15**. Rather than phenol and MBA, followed by saturation products of phenol and secondary reaction products of MBA, the NaOH-catalyzed system gave primarily phenol and phenylethanediol, with some undesired dimer products but without any further saturation products. Monomer levels fluctuated between 60-70 wt% without catalyst. Ni/HZSM-5 catalyzed reactions generated 75% total monomers early in the reaction, but secondary reactions led to subsequent monomer consumption. This confirmed that Ni/HZSM-5 is active in this system.

The reaction schemes proposed in **Fig. 17** are consistent with the products identified and suggest two important conclusions. The first being that Ni/HZSM-5 remains active in alkaline solution, and is able to exhibit catalytic activity characteristic of nickel catalysis, including both hydrogenolysis and hydrogenation, as demonstrated by the unique presence of un-oxidized cleavage products (**Fig. 17b**). The second is that both Ni/HZSM-5 and NaOH participate in the cleavage of lignin type linkages. This, along with the ability to solubilize the lignin in an alkaline solution, makes the alkaline Ni/HZSM-5 system a potential candidate for depolymerization of lignin into monomers.

4. Conclusions

All the Ni(x)/HZSM-5 catalysts in this study were able to perform HDO of guaiacol to varying extents. Furthermore, the combined functionality of Ni/HZSM-5 was shown to perform both nickel and acid catalyzed reactions, as well as facilitate reaction pathways that were not evident with Ni/SiO_2. The mixture of nickel species resulting from the DP method allowed for a few different reaction mechanisms to occur during the guaiacol HDO reaction, while the presence of HZSM-5 allowed more complete HDO through dehydration reactions and facilitated an alternate direct deoxygenation pathway.

The guaiacol HDO catalyst assays indicated that the Ni(15)/HZSM-5 catalyst with a DP time of 16 h and calcined at 673 K had the highest selectivity for HDO products, the highest nickel dispersion, and the smallest particle size. It had higher selectivity toward cyclohexane, with less accumulation of 2-methoxycyclohexanol, suggesting that it can perform direct deoxygenation on various lignin-type substituents. While the Ni/HZSM-5 catalysts prepared in these studies were able to completely deoxygenate the guaiacol model compound, all the guaiacol molecules also underwent complete saturation of the aromatic ring, which was undesirable. However, this ring saturation is most likely a result of using the simplified model compound in an organic solvent system instead of using a larger, more complex compound in an aqueous environment.

Exposing the Ni(15)/HZSM-5 DP16_Cal673 catalyst to a lignin model compound (PPE) in aqueous environments produced ethylbenzene and phenol (~35% and 23%, respectively) as its two main products, with a low extent of ring saturation compared to reactions in a non-polar, organic solvent, and a low yield of recombination products as compared with HZSM-5 in water. This selectivity towards aromatic compounds (~60%), with minimal selectivity for ring saturation and recombination reactions (both less than 10%) is important for the valorization of lignin since some of the issues that plague many lignin depolymerization technologies include oversaturation of the aromatic structure and char/coke formation (as a result of uncontrolled recombination reactions). PPE reactions with Ni/HZSM-5 in the alkaline aqueous system also exhibited promising results for β-O-4 cleavage but resulted in oversaturation of the aromatic monomers. While this is undesired, this may not occur with more complex substrates, as in the case of lignin. Also, the presence of NaOH may be necessary for the solubilization of lignin prior to reaction. This Ni/HZSM-5 catalyst prepared by a modified DP method, was able to avoid the mentioned undesired pathways while using a relatively low reaction temperature in aqueous environments (particularly in pure water), which makes this a promising catalyst system for lignin depolymerization into aromatic monomers.

5. Nomenclature

D_p particle diameter (Å)
λ CuKα radiation wavelength (Å)
$\beta_{1/2}$ full width at half maximum (radians)
θ Bragg angle (radians)
D(%) dispersion (%)
d_p particle diameter (nm)
I_R intrinsic rate (molecules of guaiacol per available nickel site) (s^{-1})
S_R specific rate ($mol \cdot g^{-1} \cdot s^{-1}$)
N_{av} Avogadro's Number
Ni_{SA} number of available nickel sites per mass of nickel (g^{-1})
Ni_{SC} number of nickel sites per mass of catalyst (g^{-1})
Ni_L nickel loading (fraction)

Acknowledgments

The work was supported by the National Institute of Food and Agriculture, U.S. Department of Agriculture, under Agreement No. 2010-38420-21828, the Project Basal PFB-27 of CONICYT, FONDECYT 1140528, and the Program PMI InEs UCO-1302 of the Chilean Ministry of Education. This work was performed in part at the Analytical Instrumentation Facility (AIF) at North Carolina State University, which is supported by the State of North Carolina and the National Science Foundation (award number ECCS-1542015). The AIF is a member of the North Carolina Research Triangle Nanotechnology Network (RTNN), a site in the National Nanotechnology Coordinated Infrastructure (NNCI). This work was also performed in part at the Environmental and Agricultural Testing Service Laboratory (EATS), Department of Crop and Soil Sciences, at North Carolina State University.

References

[1] F. G. Calvo-Flores, J. A. Dobado, ChemSusChem 2010, 3 (11), 1227-1235.

[2] J. Zakzeski, P. C. A. Bruijnincx, A. L. Jongerius, B. M. Weckhuysen, Chem. Rev. 2010, 110 (6), 3552-3599.

[3] U.S. Department of Energy. 2011, R.D. Perlack and B.J. Stokes (Leads), ORNL/TM-2011/224. Oak Ridge National Laboratory, Oak Ridge, TN.

[4] J. J. Bozell, J. E. Holladay, D. Johnson, J. F. White, Top Value Added Chemicals from Biomass. Volume II, Pacific Northwest National Laboratory, Richland, WA, PNNL-16983 (2007).

[5] M. P. Pandey, C. S. Kim, Chem. Eng. Technol. 2011, 34 (1), 29-41.

[6] P. Azadi, O. R. Inderwildi, R. Farnood, D. A. King, Renewable and Sustainable Energy Reviews 2013, 21, 506-523.

[7] A. J. Ragauskas, G. T. Beckham, M. J. Biddy, R. Chandra, F. Chen, M. F. Davis, B. H. Davison, R. A. Dixon, P. Gilna, M. Keller, P. Langan, A. K. Naskar, J. N. Saddler, T. J. Tschaplinski, G. A. Tuskan, C. E. Wyman, Science 2014, 344 (6185).

[8] R. R. Barton, M. Carrier, C. Segura, J. L. G. Fierro, N. Escalona, S. W. Peretti, Applied Catalysis A: General 2017, 540, 7-20.

[9] C. Zhao, S. Kasakov, J. He, J. A. Lercher, Journal of Catalysis 2012, 296, 12-23.

[10] C. Zhao, J. A. Lercher, Angewandte Chemie 2012, 124 (24), 6037-6042.

[11] W. Song, C. Zhao, J. A. Lercher, Chemistry – A European Journal 2013, 19 (30), 9833-9842.

[12] J. He, C. Zhao, J. A. Lercher, J. Am. Chem. Soc. 2012, 134 (51), 20768-20775.

[13] J. He, C. Zhao, D. Mei, J. A. Lercher, Journal of Catalysis 2014, 309, 280-290.

[14] W. Song, Y. Liu, E. Barath, C. Zhao, J .A. Lercher, Green Chem. 2015, 17 (2), 1204-1218.

[15] P. Burattin, M. Che, C. Louis, The Journal of Physical Chemistry B 1998, 102 (15), 2722-2732.

[16] P. Burattin, M. Che, C. Louis, The Journal of Physical Chemistry B 2000, 104 (45), 10482-10489.

[17] A. B. Dongil, I. T. Ghampson, R. Garcia, J. L. G. Fierro, N. Escalona, RSC Advances 2016, 6 (4), 2611-2623.

[18] A. L. Jongerius, R. W. Gosselink, J. Dijkstra, J. H. Bitter, P. C. A. Bruijnincx, B. M. Weckhuysen, ChemCatChem 2013, 5 (10), 2964-2972.

[19] Z. He, X. Wang, Frontiers of Chemical Science and Engineering 2014, 8 (3), 369-377.

[20] M. Lu, J. Zhu, M. Li, Y. Shan, M. He, C. Song, Energy Fuels 2016, 30 (8), 6671-6676.

[21] J. He, L. Lu, C. Zhao, D. Mei, J. A. Lercher, Journal of Catalysis 2014, 311, 41-51.

[22] J. Kong, B. Li, C. Zhao, RSC Advances 2016, 6 (76), 71940-71951.

[23] X. Wang, R. Rinaldi, ChemSusChem 2012, 5 (8), 1455-1466.

[24] S. K. Singh, J. D. Ekhe, RSC Advances 2014, 4 (53), 27971-27978.

[25] H. Konnerth, J. Zhang, D. Ma, M. H. G. Prechtl, N. Yan, Chemical Engineering Science 2015, 123, 155-163.

[26] R. Nares, J. Ramírez, A. Gutiérrez-Alejandre, C. Louis, T. Klimova, The Journal of Physical Chemistry B 2002, 106 (51), 13287-13293.

[27] C. H. Bartholomew, R. J. Farrauto, Journal of Catalysis 1976, 45 (1), 41-53.

[28] J. T. Richardson, R. J. Dubus, Journal of Catalysis 1978, 54 (2), 207-218.

[29] J. S. Smith, P. A. Thrower, M. A. Vannice, J. Catal., 1981, 68 (2), 270-285.

[30] R. Cid, G. Pecchi, Applied Catalysis 1985, 14, 15-21.

[31] J. M. Nichols, L. M. Bishop, R. G. Bergman, J. A. Ellman, J. Am. Chem. Soc. 2010, 132 (36), 12554-12555.

[32] N. Escalona, W. Aranzaez, K. Leiva, N. Martínez, G. Pecchi, Applied Catalysis A: General 2014, 481, 1-10.

[33] K. Leiva, C. Sepúlveda, R. García, J. L. G. Fierro, N. Escalona, Catalysis Communications 2014, 53, 33-37.

[34] M. Che, C. O. Bennett, In Advances in Catalysis, D.D. Eley, H. P.; Paul, B. W., Eds. Academic Press: 1989; (36), 55-172.

[35] S. Qiu, Y. Xu, Y. Weng, L. Ma, T. Wang, Catalysts 2016, 6 (9), 134.

[36] S. Kasakov, H. Shi, D. M. Camaioni, C. Zhao, E. Barath, A. Jentys, J. A. Lercher, Green Chem. 2015, 17 (11), 5079-5090.

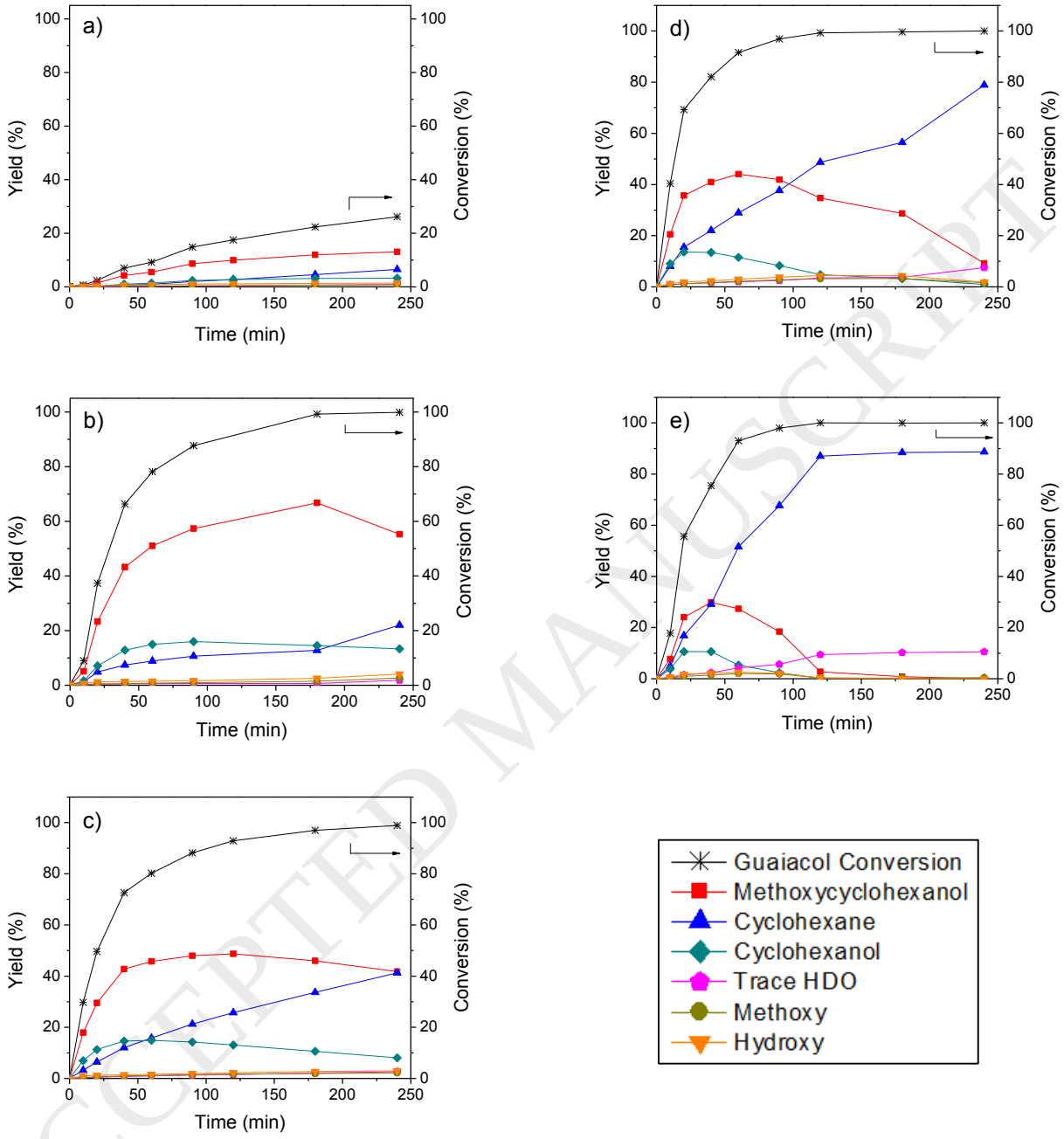

Fig. 1. Conversion of guaiacol and yield of products as a function of reaction time for a) Ni(5)/HZSM-5, b) Ni(10)/HZSM-5, c) Ni(12.5)/HZSM-5, d) Ni(15)/HZSM-5, and e) Ni(20)/HZSM-5. List of compounds for Trace HDO, Methoxy and Hydroxy categories can be found in **Fig. S16** in the supplementary material.

(Print with color)

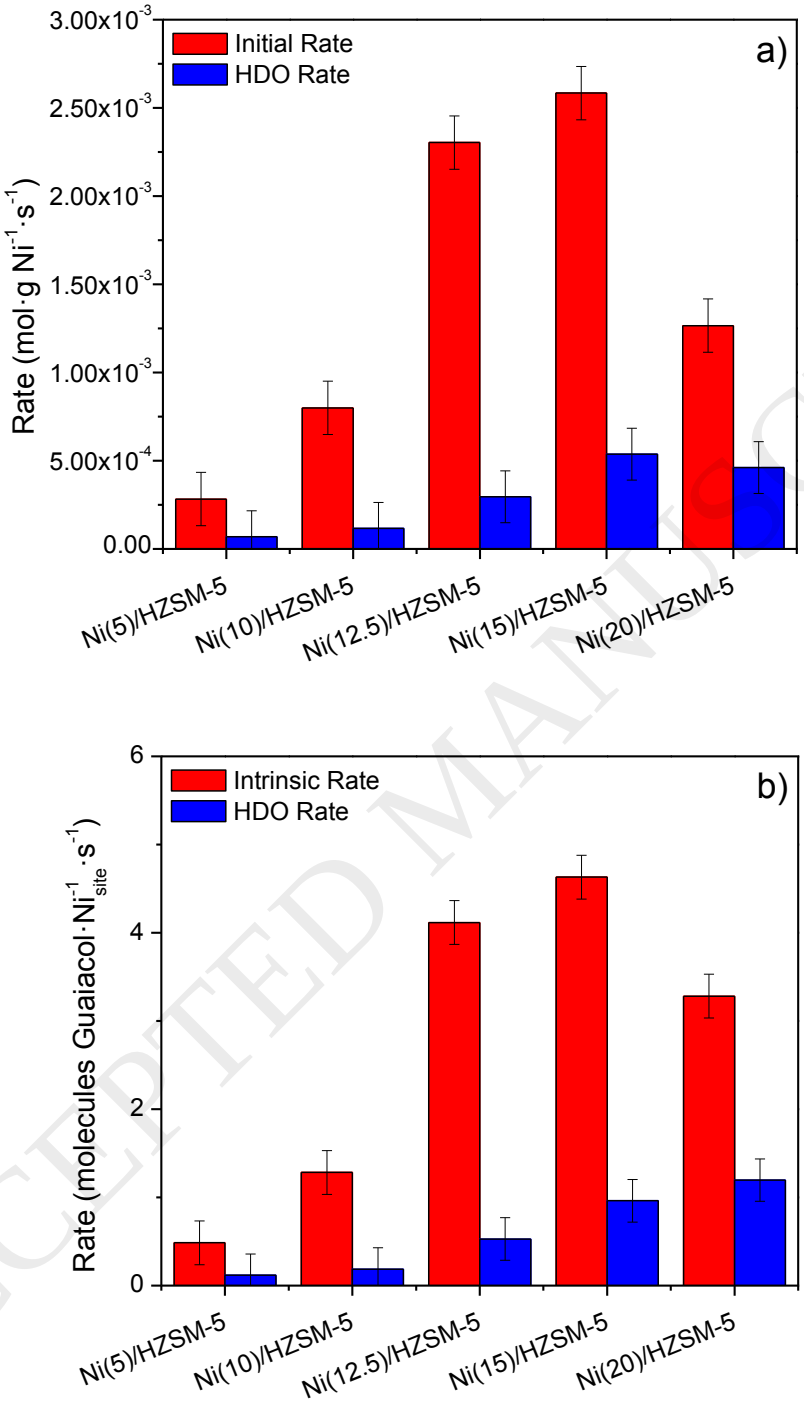

Fig. 2. a) Specific conversion and HDO rates and b) intrinsic conversion and HDO rates for Ni(x)/HZSM-5 catalysts.

(Print with color)

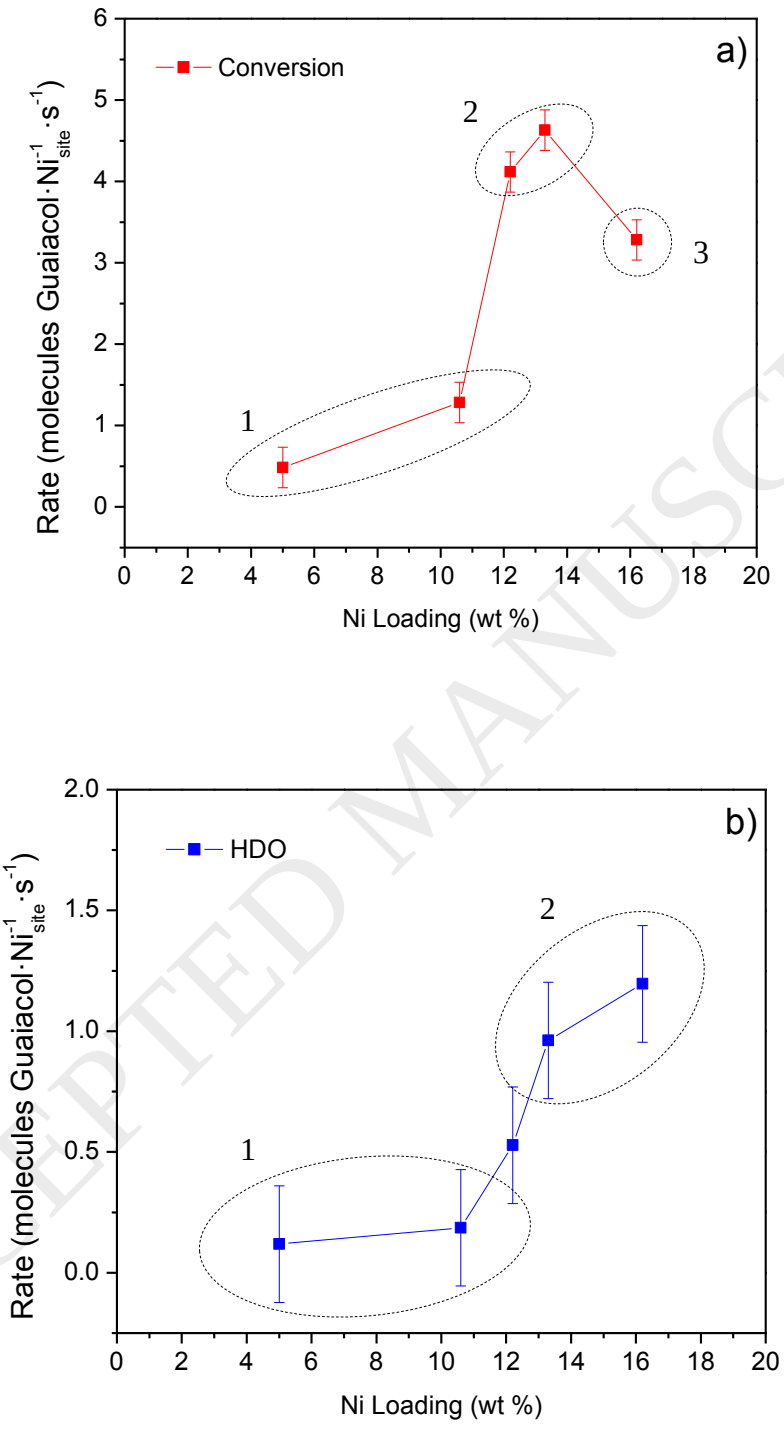

Fig. 3. Plots of intrinsic rate against nickel loading; a) guaiacol conversion, b) HDO.
(Print with color)

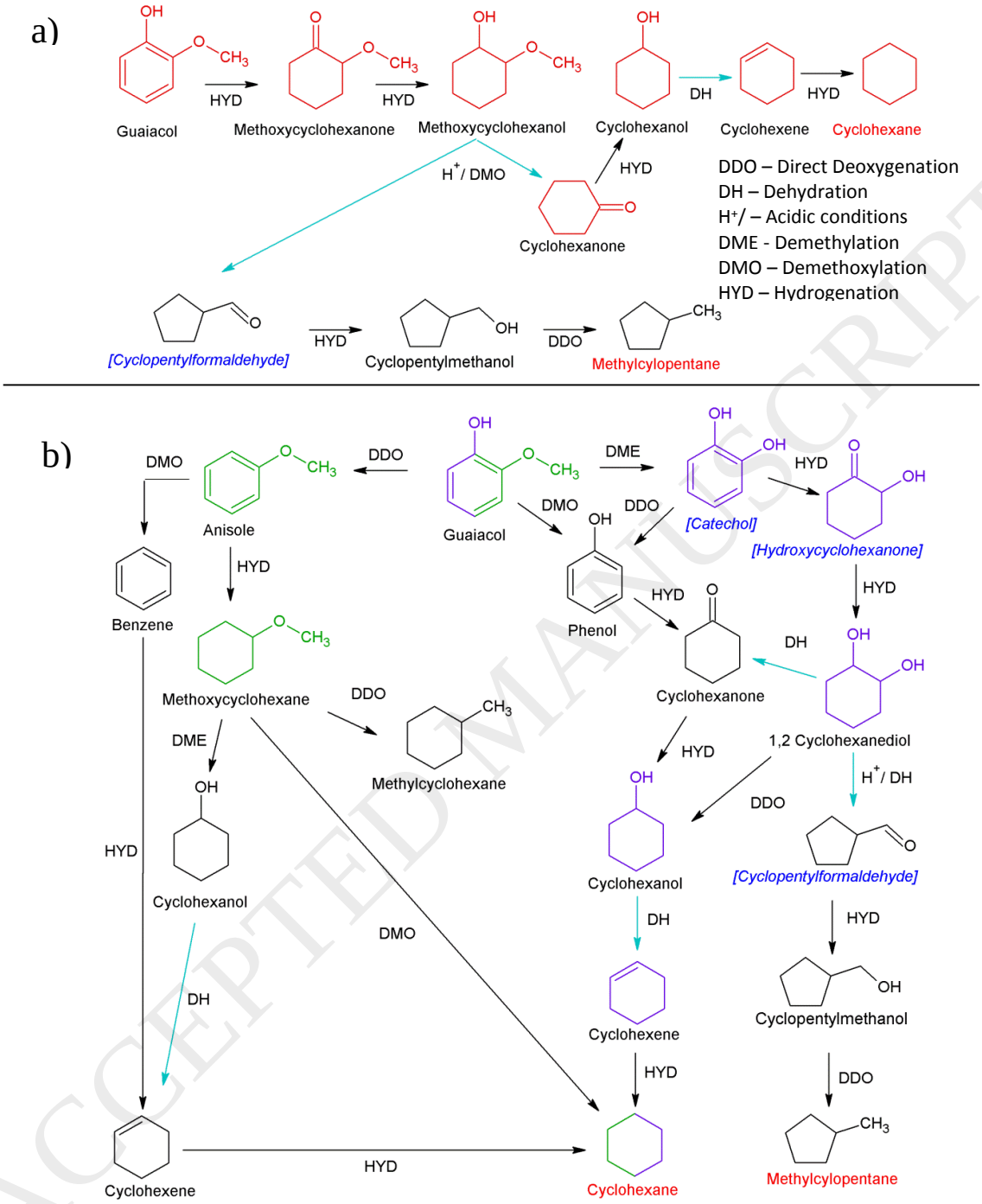

Fig. 4. Reaction network for guaiacol conversion; a) main pathways, b) alternate pathways: (⟶) nickel catalysis, (⟶) acid catalysis; Observed Product, Final Product, *[Theoretical Intermediate]*; Dominant pathway represented by dark red molecules, alternate pathway 1 is represented by purple molecules, alternate pathway 2 is represented by green molecules.

(Print with color)

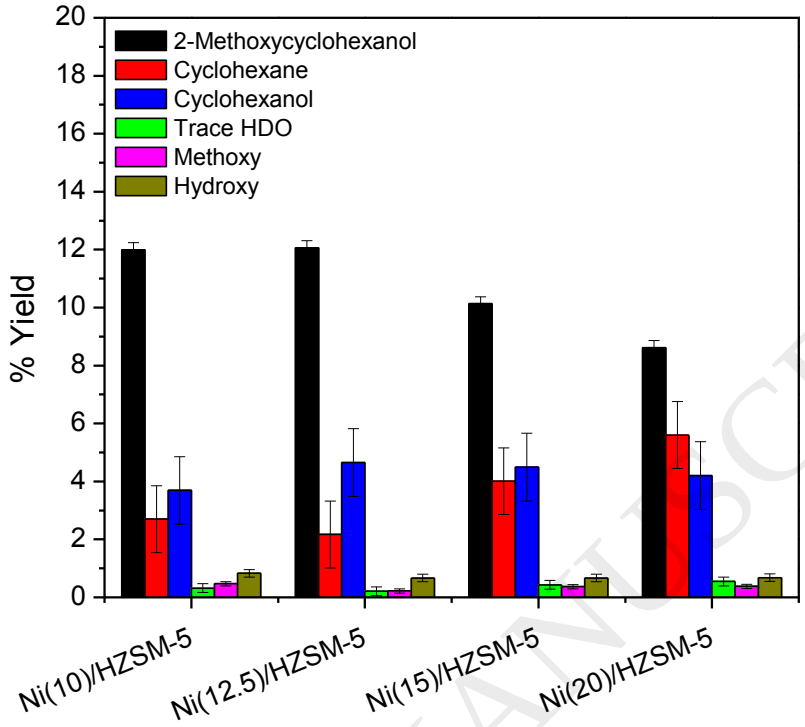

Fig. 5. Product distribution at 20% conversion of guaiacol for Ni(x)/HZSM-5 catalysts.

(Print with color)

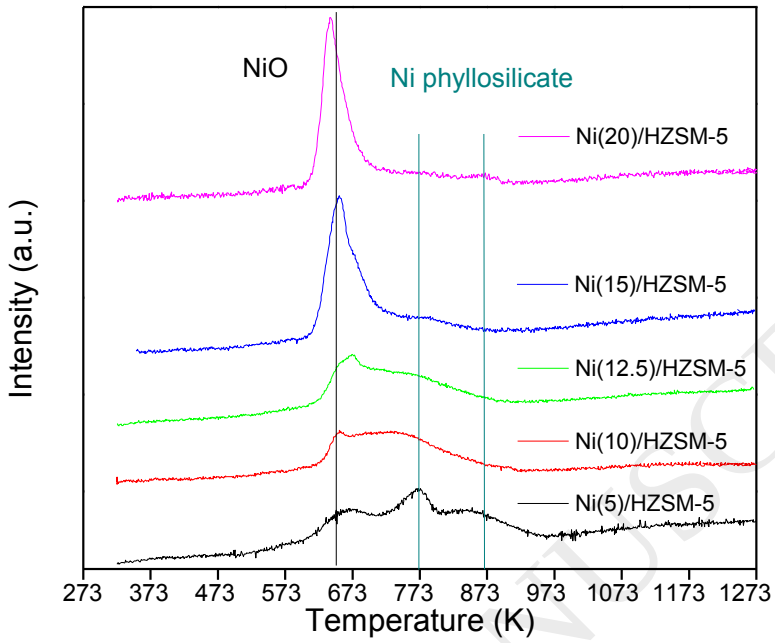

Fig. 6. Temperature programmed reduction (TPR) for Ni(x)/HZSM-5 catalysts [8].

(Print with color)

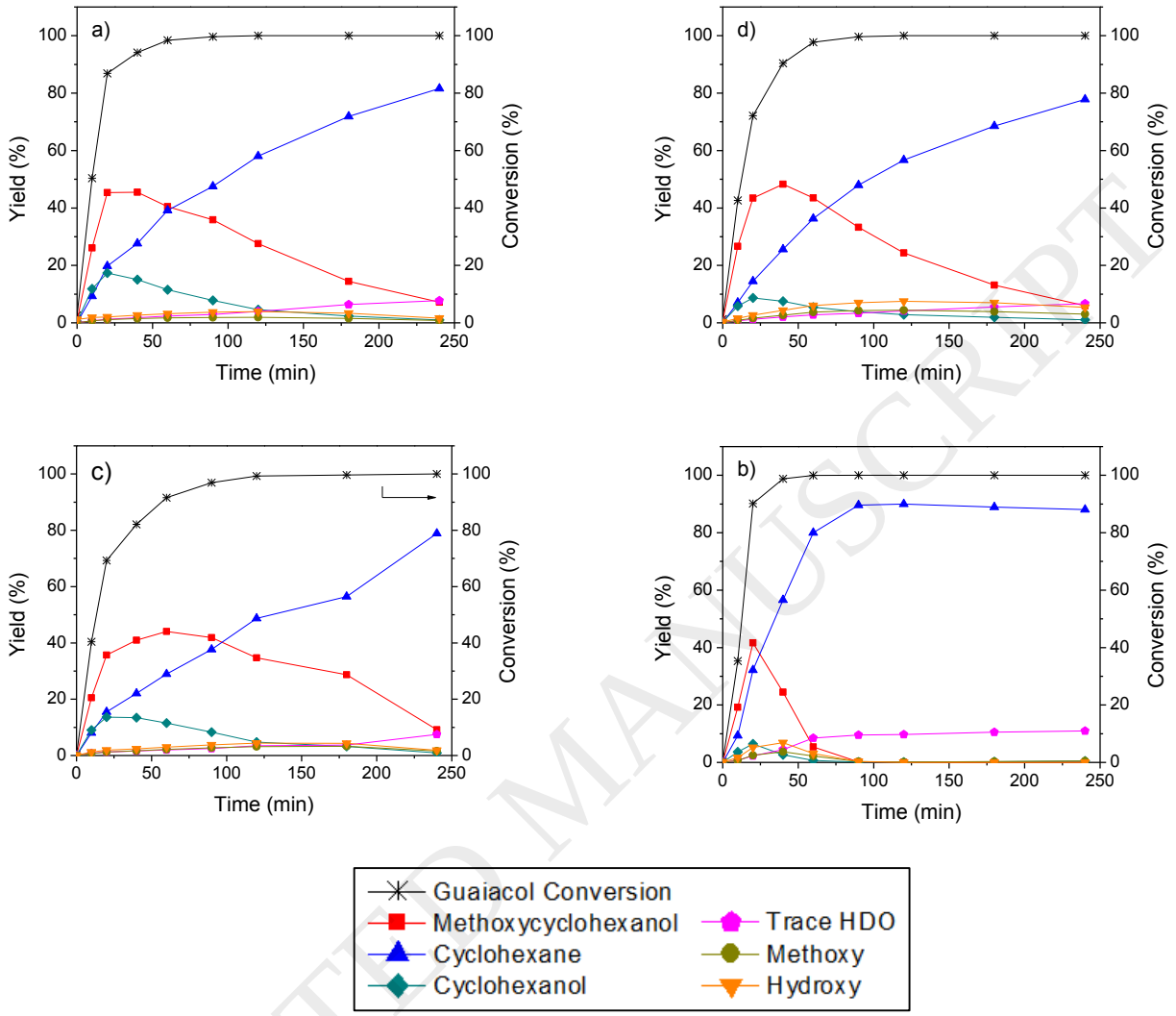

Fig. 7. Conversion of guaiacol and yield of products as a function of reaction time for Ni(15)/HZSM-5 catalysts a) DP5_Cal673, b) DP16_Cal673, c) DP5_Cal873, and d) DP16_Cal873. List of compounds for Trace HDO, Methoxy and Hydroxy categories can be found in **Fig. S16** in the supplementary material.

(Print with color)

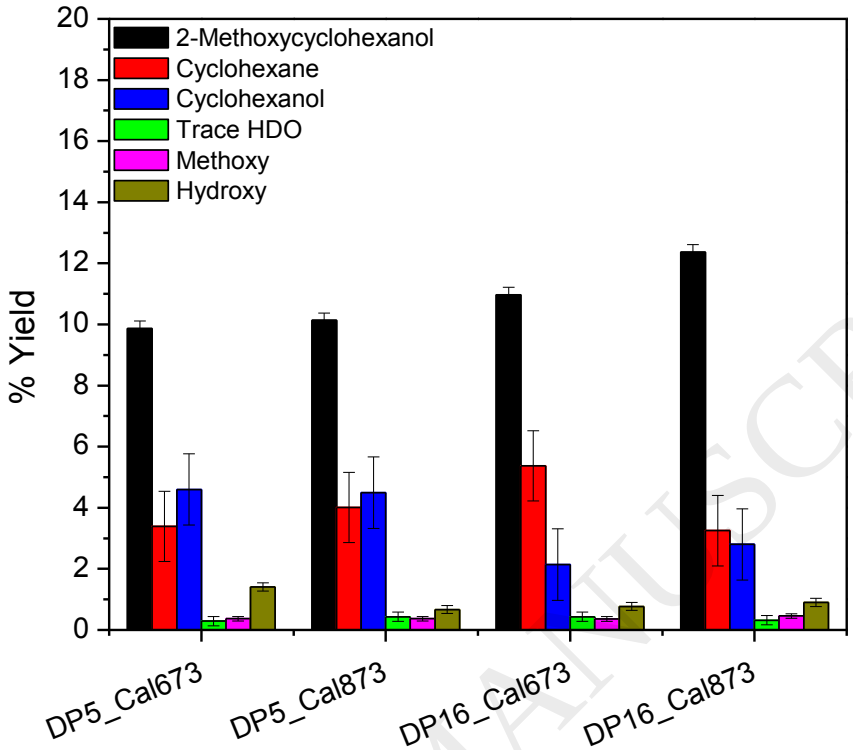

Fig. 8. Product distribution at 20% conversion of guaiacol for Ni(15)/HZSM-5 catalysts.

(Print with color)

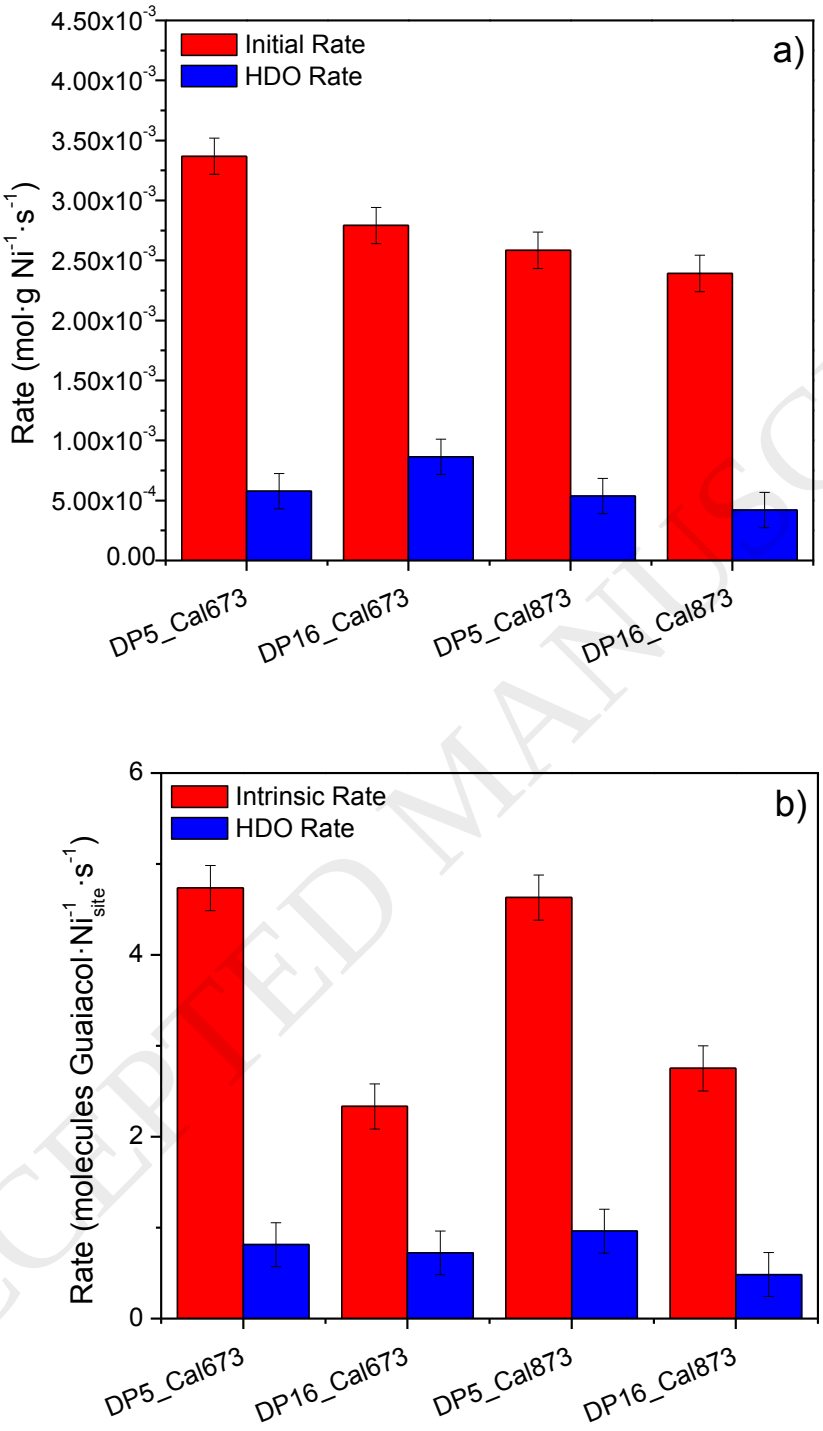

Fig. 9. a) Specific conversion and HDO rates and b) intrinsic conversion reaction and HDO rates for Ni(15)/HZSM-5 catalysts.

(Print with color)

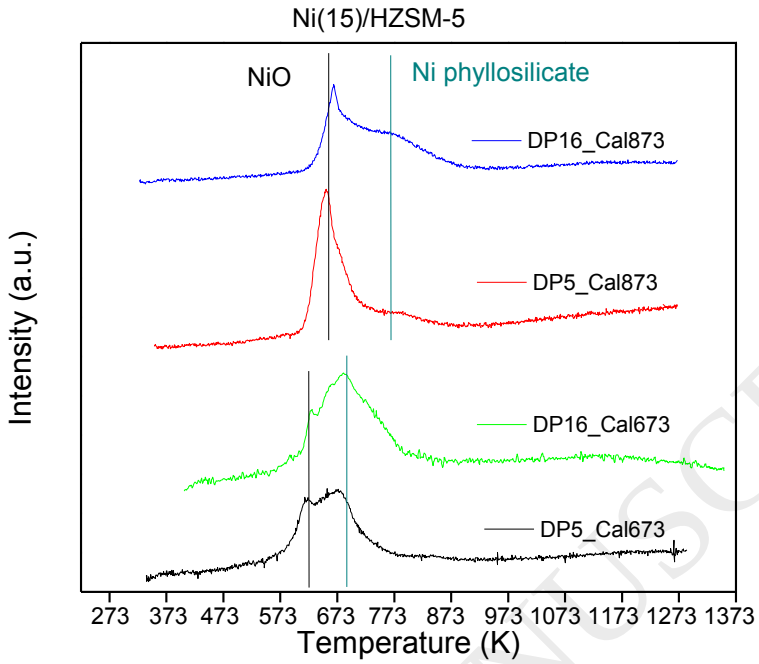

Fig. 10. Temperature programmed reduction (TPR) for Ni(15)/HZSM-5 catalysts [8].

(Print with color)

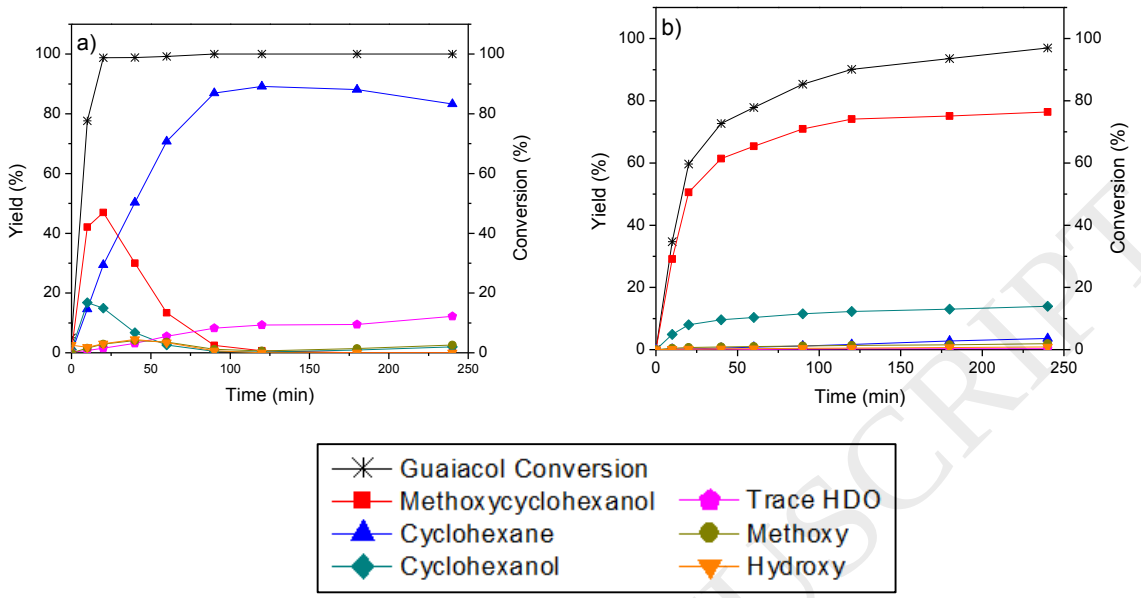

Fig. 11. Conversion of guaiacol and yield of products as a function of reaction time for a) Ni/HZSM-5 (15 wt%, DP16_Cal673) and b) Ni/SiO_2 (7 wt%), DP16_Cal673). List of compounds for Trace HDO, Methoxy and Hydroxy categories can be found in **Fig. S16** in the supplementary material.

(Print with color)

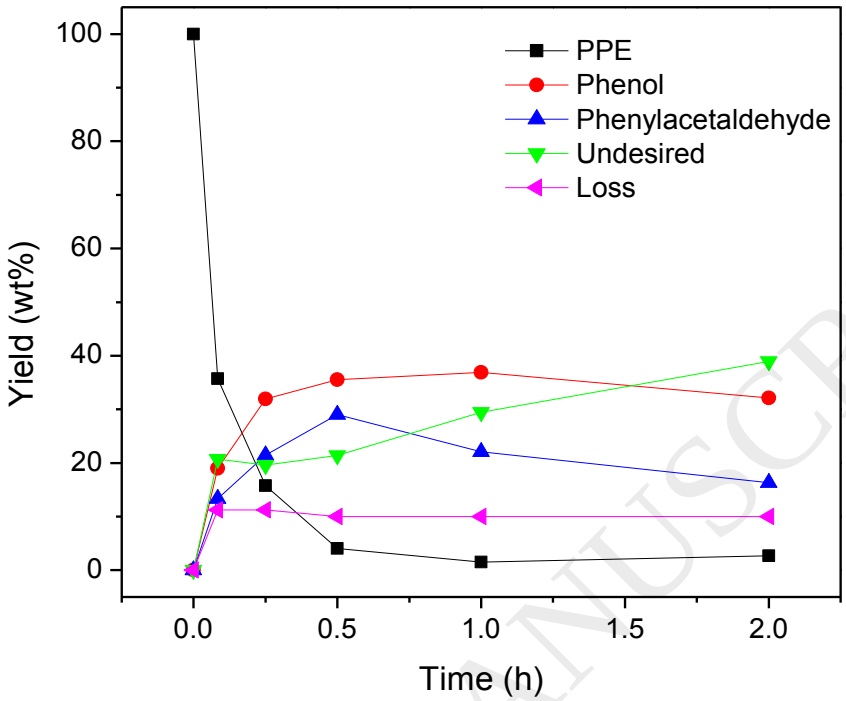

Fig. 12. Reaction progress for PPE reaction at 523 K and 5 MPa H_2, in water with HZSM-5. List of compounds for the Undesired category can be found in **Fig. S16** in the supplementary material.

(Print with color)

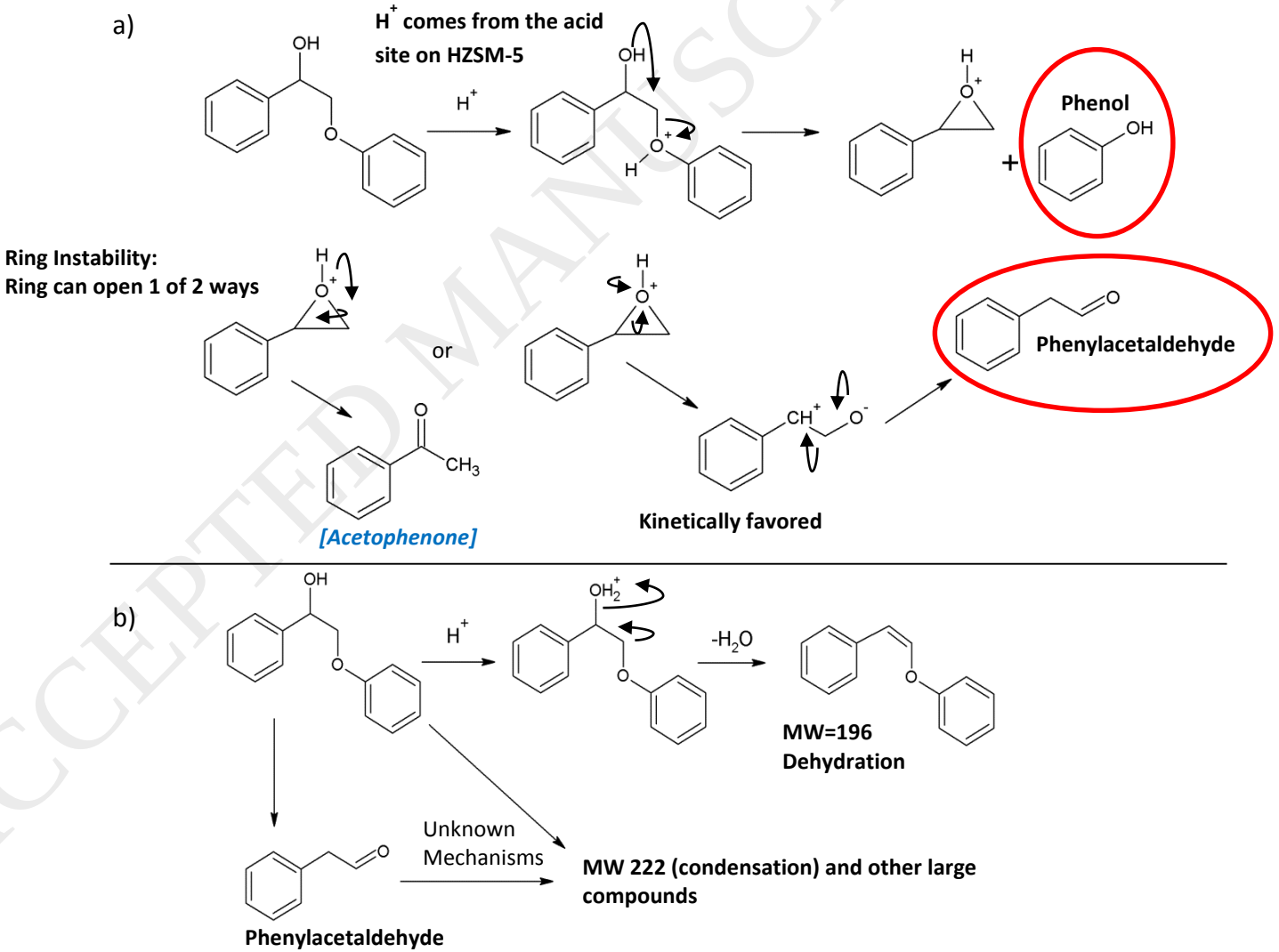

Fig. 13. PPE β-O-4 cleavage reaction mechanisms via HZSM-5 in water: a) desired product mechanisms, b) undesired product mechanisms. The acetophenone was not observed (*Theoretical*), but is a typical cleavage product of PPE.
(Print with color)

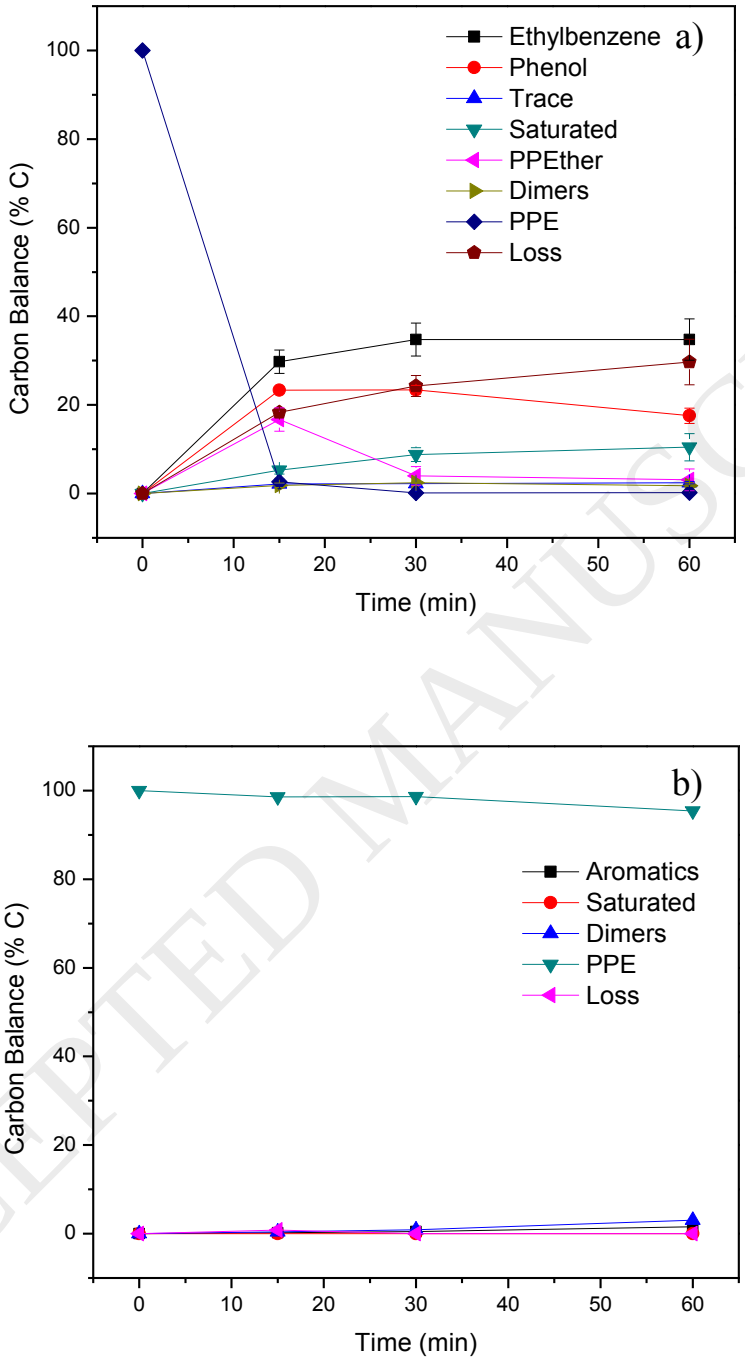

Fig. 14. Reaction progress for PPE reaction at 523 K and 5 MPa H_2, in water: a) with Ni/HZSM-5, b) without HZSM-5. List of compounds for Trace, Saturated, Dimers, and Aromatics categories can be found in **Fig. S16** in the supplementary material.

(Print with color)

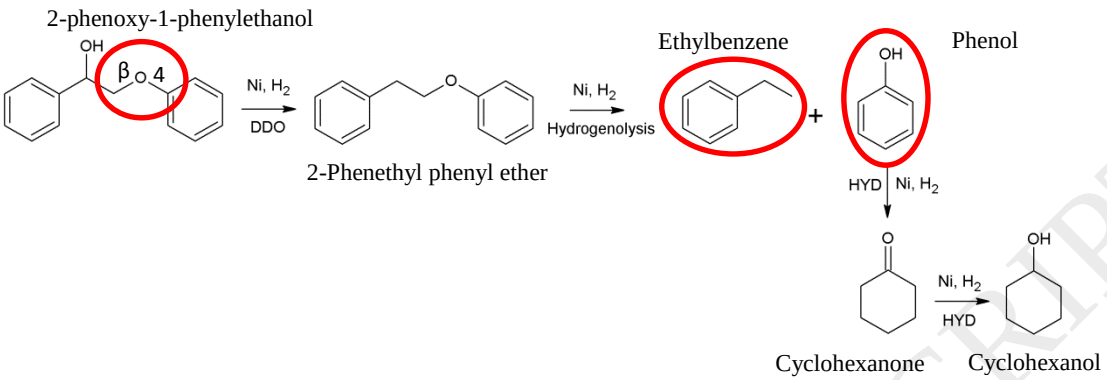

Fig. 15. PPE β-O-4 cleavage reaction mechanisms via Ni/HZSM-5 in water.

(Print with color)

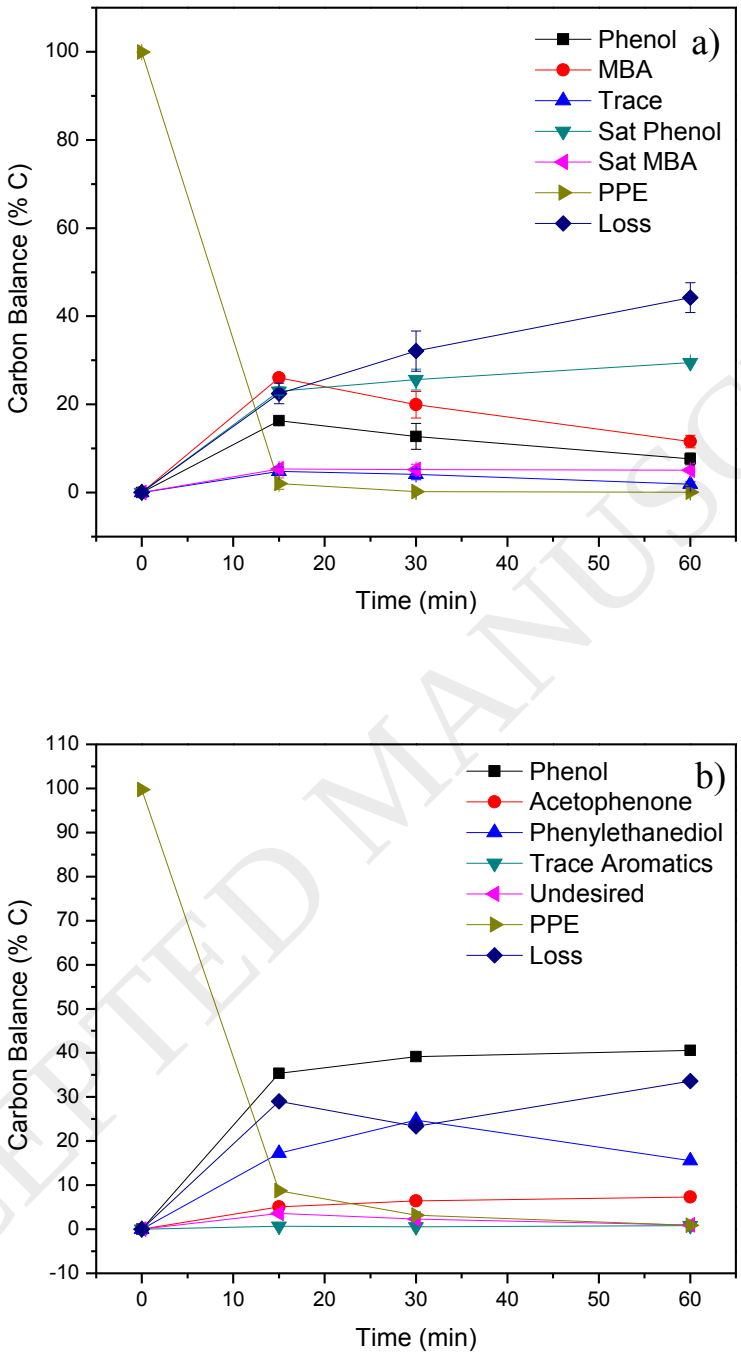

Fig. 16: Reaction progress for PPE reaction at 523 K and 5 MPa H_2, in 0.1M NaOH: a) with Ni/HZSM-5, b) without Ni/HZSM-5. List of compounds for Trace, Sat Phenol, Sat MBA, Trace Aromatics, and Undesired categories can be found in **Fig. S16** in the supplementary material.

(Print with color)

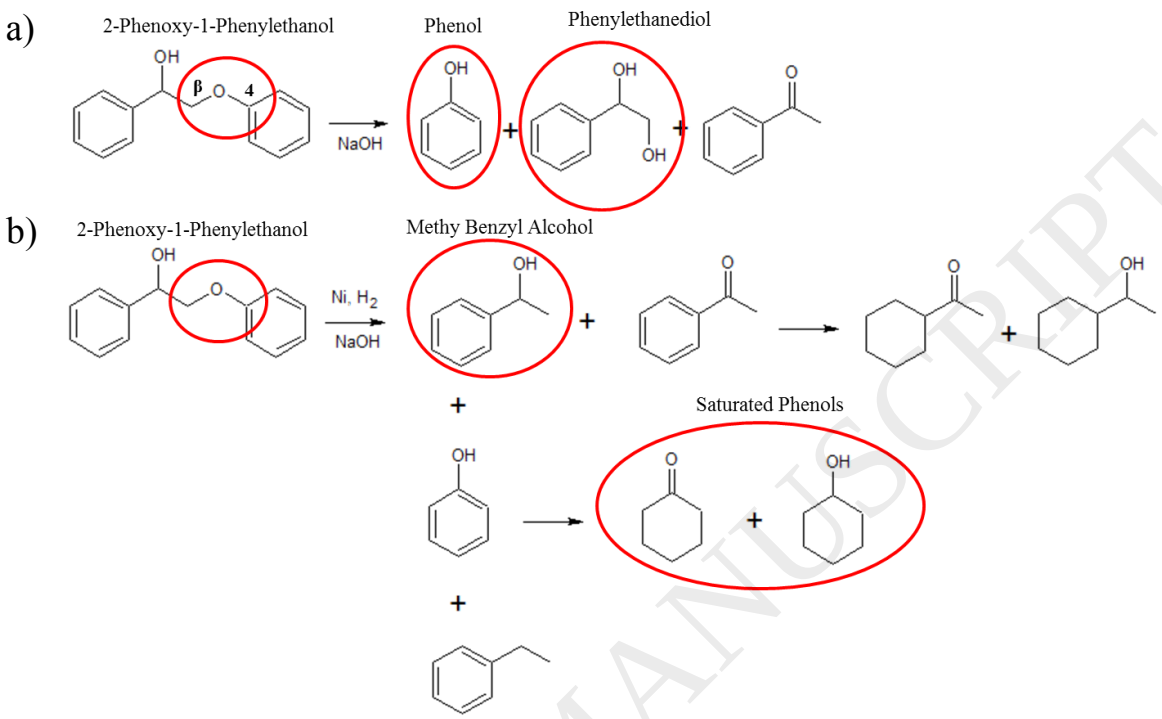

Fig. 17: PPE in 0.1 M NaOH reaction mechanisms: a) reaction without Ni/HZSM-5, b) reaction with Ni/HZSM-5.

(Print with color)

Table 1
Summary of catalyst properties for (A) varying nickel loading (5% - 20%), and (B) varying preparation conditions [8].

Catalyst	Ni Content[a] (%)	Nickel particle size (nm)			Ni Dispersion (%)	S_{BET}[c] ($m^2 \cdot g^{-1}$)	V_p[d] ($cm^3 \cdot g^{-1}$)	V_{micro}[e] ($cm^3 \cdot g^{-1}$)
		TEM	XRD	Chem.[b]				
HZSM-5	--	--	--	--	--	420	0.22	0.18
(A) Catalysts were calcined at 873 K and reduced at 733 K								
Ni(5)/HZSM-5	5.0	14±6	22	29	3.4	247	0.13	0.12
Ni(10)/HZSM-5	10.6	8±3	10	28	3.7	254	0.14	0.12
Ni(12.5)/HZSM-5	12.2	9±2	10	31	3.3	325	0.20	0.15
Ni(15)/HZSM-5	13.3	8±3	8	31	3.3	298	0.18	0.15
Ni(20)/HZSM-5	16.2	10±4	13	45	2.3	242	0.13	0.11
(B) Catalysts were loaded at 15 wt% and reduced at 733 K								
DP5_Cal673	13.3	9±3	8	24	4.2	338	0.19	0.16
DP5_Cal873	13.3	8±3	8	31	3.3	298	0.18	0.15
DP16_Cal673	14.4	5±2	7	14	7.0	253	0.18	0.11
DP16_Cal873	14.4	9±3	8	20	5.1	304	0.21	0.15

a Content determined by ICP-OES
b H_2-Chemisorption
c S_{BET} = BET surface area (N_2 adsorption)
d V_p = total pore volume
e V_{micro} = micropore volume

Table 2
XPS binding energies (eV) and surface atomic ratios for reduced Ni(x)/HZSM-5 catalysts after exposure to air [8].

Catalyst	Si 2p	Ni $2p_{3/2}$				Ni/Si
		Ni (eV)	% Reduced	NiO (eV)	% Unreduced	
(A) Catalysts were calcined at 873 K and reduced at 733 K						
Ni(5)/HZSM-5	103.3	852.4	65	854.7	35	0.306
Ni(10)/HZSM-5	103.2	852.2	74	854.6	26	1.115
Ni(12.5)/HZSM-5	103.2	852.0	58	854.2	42	1.178
Ni(15)/HZSM-5	103.3	852.2	61	854.4	39	1.425
Ni(20)/HZSM-5	103.3	852.2	70	855.3	30	2.169
(B) Catalysts were loaded at 15% and reduced at 733 K						
DP5_Cal673	103.1	852.1	72	854.4	28	1.384
DP5_Cal873	103.3	852.2	61	854.4	39	1.425
DP16_Cal673	103.3	852.3	24	854.7	76	1.444
DP16_Cal873	103.3	852.2	32	855.0	68	1.480

Table 3
Properties of the HZSM-5 and Ni/HZSM-5 catalysts used for PPE cleavage reactions.

Zeolite	SiO_2/Al_2O_3	S_{BET} ($m^2 \cdot g^{-1}$)	Pore Volume ($cm^3 \cdot g^{-1}$)
Mobil HZSM-5[a]	22	382	0.18
Zeolyst HZSM-5[b]	20	407	0.21

Catalyst[c]	Ni Content[d] (%)	Nickel particle size (nm)			Ni Dispersion (%)
		TEM	XRD	H_2-Chemisorption	
Ni(15)/HZSM-5	14.3	5±2	9	15	6.9

a Used directly for PPE reactions
b Used for Ni/HZSM-5 synthesis
c Before DP method, the zeolite was calcined at 673 K, after DP calcined at 673 K, then reduced at 733 K
d Content determined by ICP-OES analysis

Table 4
Ratio of HDO intrinsic rate to overall conversion intrinsic rate of guaiacol in dodecane at 523 K for all 15 wt % nickel catalysts.

Catalysts	HDO to Conversion Ratio (Intrinsic Rates)
DP5_Cal673	0.17
DP16_Cal673	0.31
DP5_Cal873	0.21
DP16_Cal873	0.18

Table 5
Acid strength and density obtained by potentiometric titration for Ni(15)/HZSM-5 DP16_Cal673 and Ni(7)/SiO_2 DP16_Cal673 catalysts, which were calcined, reduced, and passivated.

Catalyst	Acid Strength, E_0 (mV)	Acid Density (mmol·m^{-2})
Ni/HZSM-5	261	0.0071
Ni/SiO_2	28	0.0066

E_0 > 100 mV = very strong acid, E_0 < -100 mV = very weak acid